A NUMERICAL STUDY OF SHOCK-INDUCED HOT SPOT GENERATION IN ENERGETIC MATERIAL

BY

YANG ZHANG

THESIS

Submitted in partial fulfillment of the requirements
for the degree of Master of Science in Aerospace Engineering
in the Graduate College of the
University of Illinois at Urbana-Champaign, 2013

Urbana, Illinois

Adviser:

Professor Thomas L. Jackson

ABSTRACT

This thesis studies the formation of hot spots in energetic materials by shock initiation. A mathematical model has been developed based on viscoplastic pore collapse mechanics. Governing equations for the condensed-phase and gas-phase dynamics are derived which contain important processes including viscoplastic heating, finite-rate reaction, mass transfer and heat exchange. The system of equations are solved with two different numerical techniques. Through integration and scaling considerations, a simplified model, referred to as the space-averaging model, is firstly introduced. This model generates efficient prediction to pore collapse and expansion by solving a set of ordinary differential equations in the gas phase. Besides, a discrete model that directly solves the partial differential governing equations for the gas-phase is also developed. Detailed information about the gas phase reaction, such as temperature, mass fraction and density distributions, can be obtained from the results.

The governing equations, together with the initial and interface conditions, are solved numerically for a series of test cases for RDX ($C_3H_6N_6O_6$) and HMX ($C_4H_8N_8O_8$). The results shows that viscoplastic heating is an effective mechanism in the ignition of shocked energetic materials. In addition, it is demonstrated that the material porosity and the initial pore size have strong influence on the hot spot formation.

To My Parents

ACKNOWLEDGMENTS

I wish to take this opportunity to thank my adviser, Professor Thomas L. Jackson, for the support, guidance and encouragement he has given me along the way. But for his guidance and insightful suggestions, I would have never accomplished this task.

My sincere thanks also goes to Professor Robert Haber, from the MechSE Department, for trusting me and giving me the opportunity to work as a Teaching Assistant to fund my graduate study. I would like to thank my group mates, Guilherme Amadio and Yuya Matsumura who along the way have provide so many constructive advice to my research.

Last but not the least, I would like to thank my family: my parents Xinhui Zhang and Li Hao. Thank you for trusting me and respecting my choice. Your love provided my inspiration and was my driving force. I owe you everything and wish I could show you just how much I love and appreciate you. Sincere thanks to all my friends and other family members for their everlasting encouragement.

This work was supported (in part) by the Defense Threat Reduction Agency, Basic Research Award # HDTRA1-13-1-0010, to the University of Illinois at Urbana Champaign.

TABLE OF CONTENTS

LIST OF NOMENCLATURE, SYMBOLS OR ABBREVIATIONS

Table 1: Nomenclature

Parameter	**Description**
A_g	Pre-exponential constant for gas-phase reaction
a	Sphere internal radius
$\dot{a}$	Condensed/gas interface velocity
b	Sphere external radius
c	Specific heat
E	Activation energy
e	Specific internal energy
h	Specific enthalpy
k	Thermal conductivity
$\dot{m}$	Interface mass flux
n	Pressure exponent of gas-phase reaction
P	Pressure
R	Gas constant
R_u	Universal gas constant
r	Radius
T	Temperature
t	Time
u	Velocity
Y	Mass fraction
$\bar{Y}$	Plastic yield strength

Table 2: Greek Symbols

Parameter	**Description**
α	Thermal diffusivity
β	Isobaric expansion coefficient
η	Co-volume
μ	Viscosity
ρ	Density
σ	Principle stress
τ	Deviatoric stress
ϕ	Porosity
Φ	Energy dissipation
$\dot{\omega}$	mass production rate

Table 3: Subscripts

Parameter	**Description**
b	Sphere external radius
c	Condensed phase
g	Gas phase
i	Interface
m	Melting point
0	Initial state
r	Radial direction
θ	Tangential direction

CHAPTER 1

INTRODUCTION

1.1 Introduction

Energetic materials are compact sources of chemical energy that are designed to decompose exceedingly quickly to very hot, high pressure gases. In most cases, they are composed of granular crystalline explosive as the main component and a few percent of polymeric binder that improves their mechanical properties. Energetic materials have both military and civilian applications, and they are playing an increasingly important role in modern engineering activities. As the performance requirement for energetic materials becomes stringent in nowadays, more and more nitramine additives and energetic polymer binders are added into the traditional composition. Two most prominent members of the nitramine class are RDX (research department explosive; $C_3H_6N_6O_6$) and HMX (high melting explosive; $C_4H_8N_8O_8$). While these additives greatly enhance the performance of energetic material, the potential for an inadvertent ignition increases, along with other issues. In this case, a comprehensive understanding of the ignition mechanics of energetic material becomes important and necessary. In addition the study in the initiation of energetic material also help assesses the necessary conditions for a normal initiation.

Various methods of ignition for energetic materials exist; purely thermal mechanisms, electrostatic impulses, and shock waves. This thesis is exclusively devoted to the study of the shock initiation mechanism, used for a large part of applications.

1.2 Shock Initiation of Energetic Material

Shock propagation through condensed-phase energetic material is a complex phenomenon involving the transmission of compressional work and kinetic energy through the media. When a shock wave passes through, the energetic material can respond in different ways depending on the intensity of the shock wave. If the impact is relatively weak, the energy transferred to the material is too small to initiate reaction and no response is recorded except for mechanical damage. If the wave strength is increased to a moderate level, chemical reactions are initiated but are quenched due to insufficient initial energy. Increasing the wave strength beyond a shock initiation threshold value results in the shock-to-detonation transition (SDT). In this case the energy contained within the wave is sufficient to support sustained chemical reactions in the compressed region. In time, the pressure builds and drives a detonation wave through the material[1].

When examining the bulk temperature in the compressed zone during the SDT process, it was found that the temperature was insufficient to start the reactions in the energetic material. I was assumed that energy was firstly concentrated into localized zones, where the temperature became high enough to start the bulk reaction. These zones are known as 'hot spots'. Bowden and Yoffe[2] were the first to suggest the existence of these hot spots. In their experiments, it was found that when a small volume of gas is compressed rapidly, a high temperature reservoir of gas can be created which may potentially heat the adjacent explosive surface to the point of auto-ignition. Doolan in his paper[1] outlined a very clear description of the modern view of shock initiation, which is classified into four stages. The first stage is during the initial shock passage into the material where energy is localized into hot spots (hot spot generation). If the size, number and intensity of hot spots are sufficient and the shock pressure is maintained for a sufficiently long period, chemical reactions are sustained and burning occurs at the hot spot sites. This represents the second stage of the process (ignition). As the hot spots are at discrete locations within the material, burning initially occurs on internal surfaces with the reaction front moving outward representing stage three (internal burning). When a reasonable proportion of the material has been consumed, the burning surface switches from internal burning to external burning (stage four). This occurs when hot spots 'burn-through'

and burning is established around each individual grain or the solid material becomes sufficiently weak and fractures under the increasing pressure into smaller burning pieces suspended in the product gases.

1.3 Hot Spot Mechanisms

Although the importance of hot spots for shock ignition in energetic material has been firmly established, the exact mechanism that causes the energy localization is not well identified. This is due to the very nature of its properties; small dimension, short duration, and high temperature. As a result, direct experimental evidence on hot spot generation is hard to obtain. A comprehensive list of hot spot mechanisms are listed as follows in Field's paper[3]:

1. Adiabatic compression of trapped gas spaces.
2. Other mechanisms involving cavity collapse such as viscous or plastic heating of the surrounding matrix material or, for very high shock collapse pressures, hydrodynamic shock focusing.
3. Friction between sliding or impacting surfaces, or between explosive crystals and/or grit particles in an explosive.
4. Localized adiabatic shear of the material during mechanical failure.
5. Viscous heating of material rapidly extruded between impacting surfaces.
6. Heating at crack tips.
7. Heating at dislocation pile-ups.
8. Spark discharge.
9. Triboluminescence discharge.
10. Decomposition, followed by Joule heating of metallic filaments.

Numerical simulations of hot spot generation, shock ignition and SDT process were also actively undergone at the same time. With the growing

understanding of hot spot generation mechanics, such models experienced a transformation from purely empirical-based models to physical-based models.

1.4 Empirical Shock Initiation Models

Empirical models do not distinguish the origin of the hot spots. They only give a generalized description of the physical and chemical processes, which are implicitly related by some simple algebraic relationships. These algebraic expressions are chosen to reproduce the empirical characteristics obtained from experiments.

The majority of the empirical models date back to the 1970's and 1980's. Since this time new experimental data, making use of advances in diagnostic techniques, has been obtained, and new ideas and hypotheses on shock initiation have emerged. Based on the degree of sophistication of the models, they can be broadly categorized as single-step or multiple-step. The former category is characterized by a single rate equation describing the progress of a single reaction variable, usually the reacted mass fraction. Examples in this category include the Forest-Fire model[4] and the Lee and Tarver Ignition and Growth model[5]. The latter category is characterized by two or more linked rate models for two or more reaction variables, and it is exemplified by the Johnson-Tang-Forest (JTF) model[6].

1.4.1 Forest-Fire Model

The Forest-Fire model is one of the first reaction rate models used to predict the response of energetic materials subjected to a sustained single shock. It has been widely applied to applications involving initiation and propagation of detonation waves in PBXs. This model is purely phenomenological. It assumes that the reaction rate to be the form:

$$R = (1 - \lambda)R_{FF}(P), \tag{1.1}$$

where λ is the fraction of reacted explosive and P is the pressure. The function $R_{FF}(P)$ is fit to Pop-plot data and the partially reacted Hugoniot.

Pop-plot data is traditionally obtained from Wedge test. In this test a

wedge of high explosive is placed in front of a planar shock wave generator and the distance that the shock runs through the wedge before detonation occurs is observed with a streak camera. In an ideal explosive the change to detonation is marked by a rapid change in shock velocity and is easily observed. By varying the initial shock pressure in the plane wave generator a plot can be made of the run distance to detonation as a function of the initial sustained shock pressure. Such a plot is known as a Pop-plot, after its originator A. Popolato. The Forest-Fire coefficients are then obtained by fitting to the Pop-plot data. In order to perform this fit several assumptions have to be made. Although some of the assumptions regarding the flow behind the shock front are overly simplistic, it appears that replacing these assumptions with more realistic expressions has little effect on the computed coefficients. Because of the relative ease in conducting the wedge test, and also in fitting the Forest-Fire coefficients to the Pop-Plot data, it is fairly easy to obtain the Forest-Fire coefficients for a number of ideal energetic materials.

Forest-Fire model assumes that the reaction of the explosive takes place across the shock front which is not in accordance with experimental data. In addition, with the reaction rate being solely dependent on local pressure, the model cannot account for the phenomenon of 'shock-desensitization'[7, 8, 9].

1.4.2 Lee and Tarver Ignition and Growth Model

The Lee-Tarver Ignition and Growth model for shock initiation of heterogeneous solid explosives was first described in 1980. The model was developed on the basis, backed by considerable experimental evidence, that one can clearly distinguish two distinct phases during shock initiation, (i) an ignition phase where hot spots are created due to shock compression, and the subsequent decomposition of the explosive in these localized heated regions, and (ii) a growth phase where the build-up of reaction occurs as the reaction grows outwards from the formed reaction rate into an ignition term and one or more growth terms.

The ignition and growth concept in the Lee-Tarver model is represented by a reaction rate equation whose terms are algebraic relationships in terms of density and pressure. These terms model the hot spot and grain burn-

ing contributions of shock initiation implicity. For example, in the original version of the model the shock initiation process is divided into an ignition phase and a single growth phase,

$$\frac{\partial F}{\partial t} = I(1-F)^x \eta^r + G(1-F)^x F^y p^z,$$
$$\eta = V_0/V_1 - 1,$$

where F is the fraction of explosive that has reacted, t is time, V_0 is the initial specific volume of the explosive, V_1 is the specific volume of the shocked, unreacted explosive, p is pressure, and I, x, r, G, y, and z are constants. The η^r term is used to investigate various hot-spot formation concepts, because η the relative compression of the unreacted explosive, can be related through the unreacted equation of state to any of the thermodynamic parameters that may be involved in the initiation process. The second term in the above equation, which describes the growth of the reaction, is the most physically justifiable one of several that were formulated. The model was later modified by the addition of an extra growth term to enable short pulse duration shock initiation experiments to be accurately modeled. Since the model is readily available, it has been embedded in many hydrocodes and has been parameterized for many explosives. Hence, the Lee-Tarver model is the most popular reactive burn model in use today.

The Lee-Tarver model has been successful at predicting run-distance to detonation (Pop-Plot) data, in-material manganin pressure gauge measurements examining growth of reaction in shock initiated explosives, corner turning data, short pulse shock initiation data, and detonation propagation and failure. Thus, there are question marks over the ability of the Lee-Tarver model to predict a wide range of phenomena with a single set of parameters, or to predict experiments outside its fitting regime. The main deficiency of the Lee-Tarver model, or any pressure-dependent reaction model, is that there is no mechanism to predict explosive behavior under double shock loading, in particular the phenomena referred to as dead pressing and shock desensitization[10].

1.4.3 The JTF Model

The JTF model attempts to include an improved description of the hot spot ignition phase in describing the shock initiation of energetic material. The model partitions the energetic material into hot spots and the balance, or remainder, of the materials. Although the authors declare that the model is an explicit hot spot model, the hot spots are defined only in a general way: there are sites within the condensed-phase material that are susceptible to mechanical simulation and have a higher local temperature than the bulk material. The ignition phase is based on a thermal explosion where the induction time is a function of temperature. Here, the temperature represents an average hot spot temperature that is dependent on the pressure of the incident shock wave. The growth phase in the model, describing the burn of the balance of the energetic material, is represented by a polynomial in pressure that is very similar to the Forest Fire reaction rate. The main advantage of the JTF model is that the ignition process includes temperature as an explicit parameter. In the model, assuming a double shock process, additional heating of the hot spot (created by the first shock wave) due to the second shock is calculated as isentropic compression. Thus, the model has the potential to describe the phenomenon of desensitization by pre-shocking. The model has been shown to match sustained shock initiation data and the essential features of shock desensitization are reproduced by the model.

1.5 Physical-Based Shock Initiation Models

Although empirical models have been widely implemented in code for simulating the ignition of energetic materials, they do not in essence address the fundamental problem of how hot spots are generated. Also, empirical models fail to distinguish the shock initiation and detonation behavior of energetic materials when its properties, such as crystal or grain size, pore size and porosity, binder material, and ambient temperature, vary. To find a better solution to these problems, sophisticated models that resolve the hot spot generation are introduced. Below, a number of physical-based models are reviewed.

1.5.1 Gas Compression Ignition Model

Bowden and Yoffe[2] were the first to show that the rapid compression of a gas pocket internal to an energetic material could lead to ignition. They proposed an ignition mechanism based on adiabatic gas compression. In this model it has been proposed that when a small volume of gas is compressed rapidly, a high-temperature reservoir of gas can be created which may subsequently heat the adjacent explosive surface to the point of auto-ignition. However, it is generally believed that the gas compression is not the controlling mechanism for hot spot formation under the usual conditions of shock initiation, except when the compression rate is relatively low compared with that of typical shock waves, and the voids are relatively large.

1.5.2 Hydrodynamic Model

Mader[11] developed a hydrodynamic model for hot spot generation, under the assumption of compressible, inviscid and nonheat conductive materials. It has been suggested that when a shock wave arrives, it accelerates the upstream surface of a cavity forward, which hits the downstream side of the cavity, producing a high impact that is amplified by convergence effects during the collapse process. In this mechanism, the heating is the result of compression in the solid phase material from shock impact. Setchell and Taylor[12] improved this model by including irreversible plastic deformation to hot spots heating during the pore collapse. They also considered the material's microstructural effects on shock sensitivity by introducing a pore size parameter and a pore spacing parameter.

1.5.3 Shear-band Model

Friction or shear stress between adjacent layers in solid materials under deformation has been suggested as a possible source of ignition. In this mechanism, known as the shear-band model, the suggested physical process is that after shock loading, the energetic material will experience a rapid deformation caused by void or density discontinuities inside. This deformation is assumed to concentrate in narrow regions, called shear bands, which the energy dissipation from plastic work and viscous work gives rise to a zone

of high temperature. Frey[13], Grady and Kipp[14], and Kipp[15], for example, have developed two-step models based on this type of mechanism. In the first step, plastic work contributes to local temperature increases in shear bands until the material reaches its melting point. Following this, the heating is essentially due to viscous processes. In these models, the local temperature increase results from the action of viscoplastic heating and conduction phenomena in the material. The existence of this phenomenon has been shown in experiments by Chaudhri[16]. Saurel and Massoni[17] have proposed a model in which the friction between binder and grains liberates enough energy to become an ignition source for solid explosives.

1.5.4 Viscoplastic Pore Collapse Model

in 1972, Carroll and Holt[18, 19] introduced the elasto-plastic hollow-sphere pore collapse concept based on Rayleigh's work[20] about fluid bubble. They have shown that under high pressure stress condition plastic deformation is much more significant that elastic and elastoplastic deformation. Khasainov *et al.*[21] then firstly applied this concept and built a viscoplastic pore collapse model to study shock initiation problem in condensed energetic material. They demonstrated that viscoplastic heating were an potential source for ignition of condensed energetic material. This was supported by Frey[13]. He investigated the effects of compression rate, pore size, and material parameters on hot spot formation, and asserted that the viscous heating became dominant when pressure stress was instantaneous, material viscosity was high and yield stress was low. In the works carried out during this time period, the pore was treated either empty or containing inert gas. In addition, the gas-phase chemistry, surface reactions, and mass transfer were not considered[22]. Khasinov *et al.*[21] then improved this model by including a simplified gas-phase chemistry and mass transfer phenomena between phases. The model of Kang *et al.*[22] made a significant progress in studying the formation and growth of hot spots in energetic material. The model carefully took into account of many important physical issues. The effects of viscoplastic heating, yield strength, pore gas pressure, finite-rate chemical reaction in the gas phase, surface reaction, phase change, and heat exchange between phases were all included. Kang's model brings out a complete description to

hot spot generation, however, it is difficult to be used in a general description of a broad class of energetic. Bonnett and Bulter[23] improved Kang's model by simplifying the chemical decomposition mechanism. Massoni[17] develops another simplification of the Kang et al. model for hot spot formation by viscoplastic pore collapse in condensed heterogeneous explosives, which extended its ability to describe detonation growth.

1.6 Thesis Outline

This thesis addresses the formation and growth of hot spots in condensed-phase energetic material that are subject to sustained shock impact. Two viscoplastic pore collapse models are developed to simulate the dynamic behavior of a void inside the material after shock initiation. In chapter 3, the first model is explained, which applies the averaging method introduced by Kang[22]. It reduces the gas-phase governing equations from PDEs to ODEs to save computational cost. Using this model, a series of cases are calculated, which give the relationships of induction time, gas-phase pressure, pore radius and density as a function of shock pressure. The second model in chapter 4 solves the the entire system of governing equations in their PDE forms. In this part, we apply second-order central difference scheme for spatial derivatives and fourth-order Runger-Kutta scheme for temporary derivatives. From the numerical solution, more detailed information such as the distribution of temperature, mass fraction and density within the pore, is obtained.

In both of these two cases, the established governing equations are solved numerically for RDX and HMX.

CHAPTER 2

PHYSICAL MODEL DESCRIPTION

Fig.2.1 illustrates the mechanisms assumed during the visoplastic pore collapse. In this figure, a and b are the inner and outer radii of the hollow sphere model. They are related through the porosity equation,

$$\phi = \left(\frac{a}{b}\right)^3. \tag{2.1}$$

Energetic material occupies the space between a and b, and the void inside a is saturated with gas. From experiment data, we can obtain the average pore size, a, and porosity, ϕ, in the bulk of the energetic material. Then, b is determined by Eqn.(2.1).

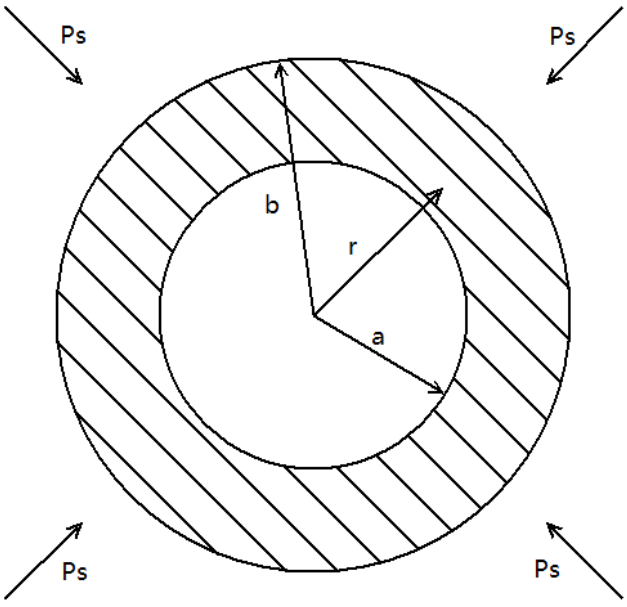

Figure 2.1: Illustration of a cross section through an idealized spherical pore. Figured based on Kang et al. (1992).

The shock is assumed to pass over the pore instantaneously, setting up a hydrostatic pressure field in the material surrounding the pore. This as-

sumption is thought to be valid for small pore sizes up to a few tens of micrometers[1].

Shock pressures experienced by energetic materials during shock initiation are usually greater than 1 GPa. In this case, the yield strength of the material is quickly overwhelmed and the pore collapses under the action of rapid viscoplastic flow. As the pore collapses, intense heating occurs near the pore surface as a result of the combined action of plastic and viscous flow. Eventually, the interface temperature increases to a level such that phase change occurs at the pore interface. We assume that sublimation occurs at the surface without condensed-phase reaction. All combustion takes place in the gas phase.

CHAPTER 3

GOVERNING EQUATIONS

In this chapter, the governing equations for the gas and solid phases are developed separately. The details of the derivation are presented as the discussion expands.

3.1 Condensed Phase

The condensed phase occupies the region $a(t) \leq r \leq b(t)$, where a and b, the inner and outer radii, are related via the porosity ϕ,

$$\phi = \left(\frac{a}{b}\right)^3, \tag{3.1}$$

and is varying with time.

Since we assume that the material in the condensed phase remains incompressible after the shock has passed, the equation for mass, momentum, and energy, assuming spherical symmetry, can be written in the following forms

$$\frac{\partial}{\partial r}(r^2 u_c) = 0, \tag{3.2}$$

$$\rho_c \left(\frac{\partial u_c}{\partial t} + u_c \frac{\partial u_c}{\partial r}\right) = \frac{1}{r^2}\frac{\partial}{\partial r}(r^2 \sigma_{rr,c}) - \frac{\sigma_{\theta\theta,c} + \sigma_{\phi\phi,c}}{r}, \tag{3.3}$$

$$\rho_c c_{v,c} \left(\frac{\partial T_c}{\partial t} + u_c \frac{\partial T_c}{\partial r}\right) = \frac{1}{r^2}\frac{\partial}{\partial r}\left(\lambda_c r^2 \frac{\partial T_c}{\partial r}\right) + \Phi_c. \tag{3.4}$$

The momentum equation, Eqn.(3.3), balances the inertial/external forces with the material stress. In this portion, the radial and tangential stress

components for total plastic flow are given by

$$\sigma_{rr,c} = -P_c - 4\mu_c \frac{u_c}{r} - \frac{2}{3}\overline{Y}\mathrm{sgn}(u_c), \tag{3.5}$$

$$\sigma_{\theta\theta,c} = \sigma_{\phi\phi,c} = -P_c + 2\mu_c \frac{u_c}{r} + \frac{1}{3}\overline{Y}\mathrm{sgn}(u_c), \tag{3.6}$$

where 'sgn' is the signum function. Since the direction of the yield stress is changing between pore collapse and expansion, by defining

$$\mathrm{sgn}(u_c) = 1 \text{ if } u_c > 0, \text{ and } \mathrm{sgn}(u_c) = -1 \text{ if } u_c < 0$$

we can retain the correct stress during the entire process.

The energy equation, Eqn.(3.4), follows the form of the energy equation for incompressible fluid, i.e., the change of internal energy, $\rho_c c_{v,c} \frac{\partial T_c}{\partial t}$, is balanced by the heat convection term, $\rho_c c_{v,c} u_c \frac{\partial T_c}{\partial r}$, the heat conduction term, $\frac{1}{r^2}\frac{\partial}{\partial r}\left(\lambda_c r^2 \frac{\partial T_c}{\partial r}\right)$, and the energy dissipation term, Φ_c. The energy dissipation term, due to viscoplastic work during pore collapse and expansion, is given by

$$\Phi_c = 12\mu_c \left(\frac{u_c}{r}\right)^2 + 2\overline{Y}\frac{|u_c|}{r}. \tag{3.7}$$

The mechanical interaction, especially the viscoplastic dissipation effect, in the condensed phase finally causes the energetic material to reach its melting temperature. At this point, the condensed phase could either melt or directly turn to gases due to its property. And the chemical reaction could take place both in the condensed and gas phases. However, for simplicity, we will ignore the melting process and only consider sublimation in this model.

The melting temperature is pressure dependent and is defined by

$$T_{\mathrm{melt}}(P_s) = T_{\mathrm{melt},0} + \beta P_s \tag{3.8}$$

3.2 Gas Phase

The gas-phase governing equations in conservative form are given by

$$\frac{\partial \rho_g}{\partial t} + \nabla \cdot (\rho_g \vec{v_g}) = 0, \tag{3.9}$$

$$\frac{\partial(\rho_g \vec{v_g})}{\partial t} + \nabla \cdot (\rho_g \vec{v_g} \vec{v_g}) = \nabla \cdot \underline{\underline{\sigma}}_g, \tag{3.10}$$

$$\frac{\partial(\rho_g e_{t,g})}{\partial t} + \nabla \cdot (\rho_g \vec{v_g} e_{t,g}) = \nabla \cdot (\underline{\underline{\sigma}}_g \cdot \vec{v_g}) - \nabla \cdot \vec{q_g}, \tag{3.11}$$

$$\frac{\partial(\rho_g Y_i)}{\partial t} + \nabla \cdot (\rho_g \vec{v_g} Y_i) = -\nabla \cdot (\rho_g Y_i \vec{V_i}) + \dot{\omega}_i. \tag{3.12}$$

The total energy is related to the internal energy via $e_{t,g} = e_g + \frac{1}{2}\vec{v_g} \cdot \vec{v_g}$. The stress tensor is given by

$$\underline{\underline{\sigma}}_g = -P\underline{\underline{I}} + \underline{\underline{\tau}}_g, \tag{3.13}$$

with $\underline{\underline{\tau}}_g$ is the viscous stress tensor. Then heat flux vector is given by

$$\vec{q_g} = -\lambda_g \nabla T + \rho_g \sum_{i-1}^{N} h_i Y_i \vec{V_i}. \tag{3.14}$$

The gas phase is completely specified given an equation of state (EOS).

3.3 Initial and Boundary Conditions

The initial conditions at $t = 0$ are given by

$$\begin{aligned} u_c = u_g &= 0, \\ P_g &= P_0, \\ T_c = T_g &= T_0, \\ Y_i &= Y_{i,0}, \\ a &= a_0, \\ b &= b_0. \end{aligned} \tag{3.15}$$

The subscript '0' denotes initial or reference states defined after the passage of a shock.

The boundary conditions at $r = b$ are given by

$$\begin{aligned} \sigma_{rr,c} &= -P_s, \\ \frac{\partial T_c}{\partial r} &= 0. \end{aligned} \tag{3.16}$$

And the boundary conditions at $r = 0$ are

$$\begin{aligned} u_g &= 0, \\ \frac{\partial u_g}{\partial r} &= 0, \\ \frac{\partial T_g}{\partial r} &= 0, \\ \frac{\partial P_g}{\partial r} &= 0, \\ \frac{\partial Y_i}{\partial r} &= 0. \end{aligned} \tag{3.17}$$

3.4 Connection Conditions

The connection conditions at the gas/condensed phase interface, $r = a$, are given by the formal representation

$$\begin{aligned} [\rho(\vec{v} - \vec{v_b}) \cdot \hat{n}] &= 0, \\ [\rho\vec{v}(\vec{v} - \vec{v_b}) \cdot \hat{n}] &= [\underline{\underline{\sigma}} \cdot \hat{n}], \\ [\rho e_t(\vec{v} - \vec{v_b}) \cdot \hat{n}] &= -[\vec{q} \cdot \hat{n}] + [(\underline{\underline{\sigma}} \cdot \vec{v}) \cdot \hat{n}] \end{aligned} \tag{3.18}$$

where $\hat{n}$ is the normal unit vector pointing into the solid.

For spherically symmetry, $\hat{n} = \hat{e}_r$ is the normal in the r-direction. The interface velocity is given by $\vec{v_b} = \dot{a}$, and thus $(\vec{v} - \vec{v_b}) \cdot \hat{n} = u - \dot{a}$, where u the velocity component in the radial direction.

The mass connection condition, assuming spherical symmetry, can be rewritten as

$$[\rho(u - \dot{a})] = 0. \tag{3.19}$$

Expanding the connection condition yields the final form

$$\rho_c(u_c|_{r=a} - \dot{a}) = \rho_g(u_g|_{r=a} - \dot{a}) = -\dot{m}, \tag{3.20}$$

where $\dot{m}$ is the mass flux.

CHAPTER 4

SPACE AVERAGING MODEL

The governing equations in the solid phase and gas phase, along with the initial, boundary, and connection conditions, form the fundamental set of equations for the proposed viscoplastic model of pore collapse. The equations are a system of partial differential equations. In order to make the numerical calculations less intensive, some simplifications can be carried out, and these are presented below.

4.1 Condensed Phase

4.1.1 Interface Motion

The interface motion can be found by solving solid-phase mass and momentum equations, subject to the mass flux and connection condition. Integrating the solid-phase continuity equation from $r = a$ to $r = b$ yields the general solution

$$u_c = \frac{f(t)}{r^2}. \tag{4.1}$$

Substituting this into the connection condition yields

$$\begin{aligned} u_c(r,t) &= \left(\frac{a}{r}\right)^2 \xi, \\ \xi(t) &= \dot{a} - \frac{\dot{m}}{\rho_c}. \end{aligned} \tag{4.2}$$

Substituting the velocity into the momentum equation, and integrating from $r = a$ to $r = b$, yields

$$\begin{aligned}&\rho_c\left(a\frac{d\xi}{dt}+2\dot{a}\xi\right)(1-\phi^{1/3})+\frac{\rho_c}{2}(u_c^2|_b-u_c^2|a)\\&=\sigma_{rr,c}|_b-\sigma_{rr,c}|_b+\int_a^b\frac{1}{r}(2\sigma_{rr,c}-\sigma_{\theta\theta,c}-\sigma_{\phi\phi,c})dr.\end{aligned}\tag{4.3}$$

Noting that

$$\begin{aligned}\sigma_{rr,c}|_b&=-P_s,\\\sigma_{rr,c}|_a&=-P_g+\dot{m}^2\left(\frac{1}{\rho_c}-\frac{1}{\rho_g}\right),\end{aligned}\tag{4.4}$$

where we neglect the gas-phase viscous stress at the interface, and

$$\int_a^b\frac{1}{r}(2\sigma_{rr,c}-\sigma_{\theta\theta,c}-\sigma_{\phi\phi,c})\,dr=-4\mu_c\frac{\xi}{a}(1-\phi)-2\overline{Y}\mathrm{sgn}(\xi)\ln\left(\frac{b}{a}\right).\tag{4.5}$$

So the equation for interface motion is

$$\boxed{\begin{aligned}\frac{d\xi}{dt}=&\frac{1}{a\rho_c(1-\phi^{1/3})}\left\{P_g-P_s-4\mu_c\frac{\xi}{a}(1-\phi)-\dot{m}^2\left(\frac{1}{\rho_c}-\frac{1}{\rho_g}\right)\right.\\&\left.-2\overline{Y}\mathrm{sgn}(\xi)\ln\left(\frac{b}{a}\right)-2\rho_c\xi\left(\xi+\frac{\dot{m}}{\rho_c}\right)\left(1-\phi^{1/3}\right)+\frac{\rho_c}{2}\xi^2\left(1-\phi^{4/3}\right)\right\}.\end{aligned}}\tag{4.6}$$

This is a second-order ODE for $a(t)$. To integrate, the initial conditions $a(0) = a_0$ and the value of $\dot{a}(0)$ are needed. Kang[22] and Massoni[7] set $\dot{a} = 0$. But the the validity of this value needs further justification, and we will give alternative options based on the simplified model developed later.

Eqn.(4.6) is solved directly by Kang[22], Massoni[17], and Doolan[1]. However, an investigation into the scaling issues shows us a further simplified way to solve interface motion. If we examine the condensed-phase momentum equation, Eqn.(3.3), we have the following balances

$$\frac{\rho_c u_c^2}{a}\sim\frac{\overline{Y}}{a}\sim\frac{P_s}{a}\sim\frac{2\mu_c u_c}{a^2}\tag{4.7}$$

In particular, if we set $a = n\times10^{-6}$m and $P_s = N\times10^{9}$Pa, the viscous-inertia

ratio is given by

$$\frac{2\mu_c u_c}{a^2} \div \frac{\rho_c u_c^2}{a} = \frac{8\mu_c^2}{\rho_c a^2 P_s} \sim \frac{(1.8)10^4}{Nn^2}; \tag{4.8}$$

similar expressions can be found for the other balances. This shows that the inertia terms are small compared to the terms on the right hand side of Eqn.(3.3) and can therefore be neglected. Therefore, neglecting the inertia terms in the integrated momentum equation (4.3), using (4.4) and (4.5), becomes

$$\boxed{0 = -P_s + P_g - 4\mu_c \frac{\xi}{a}(1-\phi) - \dot{m}^2 \left(\frac{1}{\rho_c} - \frac{1}{\rho_g}\right) - 2\overline{Y}\,\mathrm{sgn}(\xi)\ln\left(\frac{b}{a}\right).} \tag{4.9}$$

4.1.2 Interface Motion prior to Melting

Prior to melting, $\dot{m} = 0$ and we ignore P_g since it is much smaller than P_c, then we get

$$0 = -P_s - 4\mu_c \frac{\dot{a}}{a}(1-\phi) + 2\overline{Y}\ln\left(\frac{b}{a}\right); \tag{4.10}$$

i.e.,

$$\frac{da}{dt} = \frac{a}{4\mu_c(1-\phi)} \left\{ -P_s + 2\overline{Y}\ln\left(\frac{b}{a}\right) \right\}. \tag{4.11}$$

The overall mass conservation, when $\dot{m} = 0$, requires that the mass balance between $r = a$ and $r = b$ remains fixed, i.e.,

$$\frac{d}{dt}(b^3) = \frac{d}{dt}(a^3). \tag{4.12}$$

Eqn.(4.11) and Eqn.(4.12) define a first-order differential equation for $a(t)$ that only need $a(0)$ for its solution.

If we note that $\phi << 1$ and that integration of Eqn.(4.12) gives $b^3 - b_0^3 = a^3 - a_0^3$, i.e.,

$$\frac{b^3}{b_0^3} = 1 - \frac{a^3 - a_0^3}{b_0^3}, \tag{4.13}$$

and recognize

$$\left| \frac{a^3 - a_0^3}{b_0^3} \right| < \frac{a_0^3}{b_0^3} < 0.05 \tag{4.14}$$

so that $b \sim b_0$ and we can replace b/a with b_0/a, then Eqn.(4.11) becomes

$$\frac{\dot{a}}{a} = -\frac{P_s}{4\mu_c} + \frac{\overline{Y}}{2\mu_c}\ln\left(\frac{b_0}{a}\right) \tag{4.15}$$

This equation can be integrated if we set $\ln(a) = f(t)$, and after some algebra we get

$$\ln\left(\frac{a}{b_0}\right) = -\frac{P_s}{2\overline{Y}} + \left(\frac{P_s}{2\overline{Y}} + ln\left(\frac{a_0}{b_0}\right)\right)\exp\left[-\frac{\overline{Y}}{2\mu_c}t\right] \tag{4.16}$$

Now we expect $t \sim O(10^{-7}s)$, $\overline{Y}t/2\mu_c \sim 0.15$, and we can approximate the exponential by a linear function of t, viz.

$$\exp\left[-\frac{\overline{Y}}{2\mu_c}t\right] \approx 1 - \frac{\overline{Y}}{2\mu_c}t. \tag{4.17}$$

Equation (30) then becomes

$$\frac{a}{a_0} = \exp\left[-t\left\{\frac{P_s}{4\mu_c} - \frac{\overline{Y}}{2\mu_c}ln\left(\frac{b_0}{a_0}\right)\right\}\right] \equiv \exp[-vt]. \tag{4.18}$$

4.1.3 Interface Motion after Melting

After melting we need to solve Eqn.(4.3) numerically. We can still make the approximations $\phi << 1$ and $b \approx b_m$ where $b_m = (a_m^3 + (b_0^3 - a_0^3))^{1/3}$ is the value of b when melting first occurs, to get

$$\frac{da}{dt} = \frac{\dot{m}}{\rho_c} - \frac{a}{4\mu_c}\left[P_s - P_g - \dot{m}^2\left(\frac{1}{\rho_g} - \frac{1}{\rho_c}\right) - 2\overline{Y}\ln\left(\frac{b_m}{a}\right)\right] \tag{4.19}$$

with condition $a(t_m) = a_m$ at $t = t_m$, the time melting first occurs.

4.1.4 Energy Equation

We next examine the energy equation in the condensed phase, Eqn(3.4). First, we examine each term in the solid-phase energy equation to determine their respective order of magnitudes. These are:

- Conductive: $\lambda_c \Delta T/a^2 = 2.0 \times 10^{14}$ kg/m-s^3
- Inertia: $\rho_c c_c U \Delta T/a = 4.5 \times 10^{16}$ kg/m-s^3

- Dissipation: $12\mu_c U^2/a^2 = 2.2 \times 10^{17}$ kg/m-s^3
- Yield: $2\overline{Y}U/a = 6.8 \times 10^{15}$ kg/m-s^3

Here, we have taken $\rho_c = 1800$ kg/m^3, $c_c = 1465$ J/kg-K, $\mu_c = 65$ kg/s-m, $a = 1.0 \times 10^{-6}$ m, $\Delta T = 1000$ K, $\lambda_c = 0.2093$ W/m-K, $P_c = 2.2$ GPa, $\overline{Y} = 0.2$ GPa, and $U = P_c a/(2\mu_c) = 16.9$ m/s. Thus, we see that the condition term is several orders of magnitude smaller than the inertia and dissipation terms, and one order of magnitude smaller than the yield term. This implies that heat conduction is only important in a narrow region about the pore surface. Also, note that

$$\text{dissipation/conduction} = 3P_c^2 a^2/(\lambda_c \mu_c \Delta T),$$

so that as P_c or a gets larger, the importance of heat conduction in the bulk of the solid diminishes. This analysis suggests we can neglect heat conduction and therefore examine the inertia and dissipation balance.

Ignoring heat conduction, the energy equation can be written as

$$\rho_c c_{v,c} \left(\frac{\partial T_c}{\partial t} + u_c \frac{\partial T}{\partial r} \right) = 12\mu_c \left(\frac{u_c}{r} \right)^2 + 2\overline{Y} \frac{|u_c|}{r}. \tag{4.20}$$

Since this equation is hyperbolic, it can be solved using the method of characteristics. The characteristics are defined by

$$\frac{dr}{dt} = u_c \tag{4.21}$$

Before melting we have $\dot{m} = 0$, so that $u_c = a^2 \dot{a}/r^2$ from (16), and hence

$$\frac{dr}{dt} = \frac{a^2 \dot{a}}{r^2}. \tag{4.22}$$

The solution to this equation is given by

$$r^3 = a^3 + (r_0^3 - a_0^3). \tag{4.23}$$

Here, r_0 is the characteristics defined at $t = 0$ and a_0 is the initial value of a. The energy equation along the characteristics is given by

$$\rho_c c_{v,c} \frac{dT_c}{dt} = \frac{12\mu_c a^4 \dot{a}^2}{[a^3 + (r_0^3 - a_0^3)]^2} + \frac{2\overline{Y} a^2 |\dot{a}|}{[a^3 + (r_0^3 - a_0^3)]}. \tag{4.24}$$

This equation must be integrated numerically along the characteristics.

4.1.5 Energy Equation prior to Melting

Prior to melting, $\dot{m} = 0$ and we let $a = a_0 e^{-vt}$, then Eqn.(4.24) has an exact solution. If we integrated using $s = a^3$ rather then t, noting that $d/dt = (d/ds)(ds/dt) = 3a^2\dot{a}(d/ds)$, Eqn.(4.24) transforms to

$$3\rho_c c_{v,c}\frac{dT_c}{ds} = -\frac{12\mu_c v s}{[s+(\alpha-1)s_0]^2} - \frac{2\overline{Y}}{[s+(\alpha-1)s_0]}, \tag{4.25}$$

where $r_0^3 = \alpha s_0$, $a_0^3 = s_0$, so that $r_0^3 - a_0^3 = (\alpha-1)s_0$. Integration yields

$$\begin{aligned} 3\rho_c c_{v,c}(T-T_0) = &-(12\mu_c\nu + 2\overline{Y})\ln\left[\frac{s+(\alpha-1)s_0}{\alpha s_0}\right] \\ &- \frac{12\mu_c\nu(\alpha-1)s_0}{s+(\alpha-1)s_0} + \frac{12\mu_c\nu(\alpha-1)}{\alpha}. \end{aligned} \tag{4.26}$$

Here, T_0 is the initial post-shock temperature. The special case $\alpha = 1$ corresponds to the interface. The interface temperature is given by

$$T_f = T_0 - \frac{12\mu_c v + 2\overline{Y}}{\rho_c c_{v,c}} ln\left(\frac{a_f}{a_0}\right), \tag{4.27}$$

where the subscript f indicate the front value. Together with $a_f = a_0 e^{-vt}$ we can determine when the front first melts, i.e., when $T_f = T_{\text{melt}}$.

4.1.6 Energy Equation after Melting

Melting first occurs when the pore surface temperature T_f reaches a high enough value. The melting temperature is a function of pressure, which is given by

$$T_m = T_{m0} + \beta P_s. \tag{4.28}$$

Once melting temperature occurs $\overline{Y} = 0$ and there is a large drop in viscosity so that one may set $\mu_c = 0$. At the same time additional physics is switched on: for example, the interface mass flux $\dot{m}$, so that at the interface the flow

speed in the condensed-phase is

$$u_{c,i} = \dot{a} - \dot{m}/\rho_c \tag{4.29}$$

and

$$u_c = (\dot{a} - \dot{m}/\rho_c)\frac{a^2}{r^2} \quad \text{in} \quad a < r < b. \tag{4.30}$$

$\dot{m}$ is a function of the interface temperature if one assumes it is created by a simple pyrolysis law.

After melting occurs at the interface a melting front $r = r_m$ moves into the interior of the condensate so that

$$\begin{aligned} T &= T_m \quad \text{when} \quad a < r < r_m \\ T &> T_m \quad \text{when} \quad r_m < r < b. \end{aligned} \tag{4.31}$$

In due course the reactive gases pumped into the pore as components of $\dot{m}$ support violent reaction and both the pore pressure and the pore temperature increase dramatically. Fortunately, the condensate interface temperature remains $T = T_m$, and this is all the information we need to solve the gas-phase thermal explosion problem, which will be discussed below.

4.2 Gas Phase

The gas phase plays no role until the solid temperature has been raised to the melting temperature, at which time reactive gases begin to fill the pore. Thus, the analysis below is valid for post-melting conditions.

4.2.1 Simplification and Averaging

The gas-phase equations can first be simplified to a set of ordinary differential equations by performing integrations over the pore volume. Condition is assumed to be unimportant in the pore, except near the interface, and so we can neglect all diffusion terms. We begin by integrating the equations (6) in

conservative form over the pore volume,

$$\begin{aligned}
\int_V \frac{\partial \rho_g}{\partial t} dV + \int_V \nabla \cdot (\rho_g \vec{v}_g) dV = 0, \\
\int_V \frac{\partial (\rho_g Y_i)}{\partial t} dV + \int_V \nabla \cdot (\rho_g \vec{v}_g Y_i) dV = \int_v \dot{\omega}_i dV, \\
\int_V \frac{\partial (\rho_g e_{t,g})}{\partial t} dV + \int_V \nabla \cdot \left(\rho_g \vec{v}_g e_{t,g} - \underline{\underline{\sigma}}_g \cdot \vec{v}_g \right) dV = 0
\end{aligned} \tag{4.32}$$

Here, we have neglected the conservation of momentum equation since in a low Mach number approximation, the only purpose of the momentum equation is to determine the $O(M^2)$ correction to the mean (thermodynamic) pressure. Also, since the Mach number is small the only term that we keep in the viscous dissipation term is

$$\underline{\underline{\sigma}}_g = -P_g \underline{\underline{I}}. \tag{4.33}$$

Here, because of the small Mach number assumption, the thermodynamic pressure is only a function of time; i.e., $P_g = P_g(t)$.

To simplify the equations we will make use of the divergence theorem

$$\int_V \nabla \cdot \vec{F} dV = \int_S \vec{F} \cdot \hat{n} dS, \tag{4.34}$$

to replace the volume integral in terms of a surface integral. Here the surface is defined at $r = a(t)$, and $\hat{n}$ is the outward pointing unit normal. We use Leibniz's rule

$$\int_{V(t)} \frac{\partial F}{\partial t} dV = \frac{d}{dt} \int_{V(t)} F dV - \int_{S(t)} F (\vec{v}_b \cdot \hat{n}) dS, \tag{4.35}$$

where $\vec{v}_b$ is the surface/boundary velocity of the pore, $V = 4\pi a^3$ the volume, and $S = 4\pi a^2$ the surface area.

We define the following quantities and averages

$$\bar{\rho}_g = \frac{M_g}{V} = \frac{\int_V \rho_g dV}{\frac{4}{3}\pi a^3}, \tag{4.36}$$

$$M_g = \int_v \rho_g dV, \tag{4.37}$$

$$\bar{Y_i} = \frac{\int_V \rho_g Y_i dV}{M_g}, \tag{4.38}$$

$$\bar{\dot{\omega}_i} = \frac{\int_V \dot{\omega}_i dV}{V}, \tag{4.39}$$

$$h_g = \sum Y_i h_{i,g} = \sum Y_i \Delta h^\circ_{i,g} + c_p T. \tag{4.40}$$

For the internal energy we write it as the sum of the sensible part plus chemical, i.e.,

$$e_g = e_{g,s} + e_{g,c}, \tag{4.41}$$

where the sensible part is defined in the usual fashion

$$e_{g,s} = h_g + P_g/\rho_g, \tag{4.42}$$

and the chemical energy is given by

$$e_{g,c} = \sum Y_i \Delta h^\circ_{i,g}. \tag{4.43}$$

4.2.2 Mass

Using the divergence theorem and Leibniz' rule the conservation of mass can be written as

$$\frac{d}{dt}\int_V \rho_g dV - \int_S \rho_g(\vec{v}_b \cdot \hat{n})dS + \int_S (\rho_g \vec{v}_g) \cdot \hat{n} dS = 0, \tag{4.44}$$

or,

$$\frac{d}{dt}\int_V \rho_g dV = \int_S \rho_g[(\vec{v}_b - \vec{v}_g) \cdot \hat{n}]dS, \tag{4.45}$$

or simply

$$\frac{dM_g}{dt} = \int_S \dot{m} dS \tag{4.46}$$

Note that on the RHS we used the connection condition $r = a$

$$\rho_g(u_{g,a} - \dot{a}) = -\dot{m} \tag{4.47}$$

with $\vec{v}_b = \dot{a}$ for the speed of the interface. Since ρ_g and $\dot{m}$ do not vary along the surface (spherical symmetry), we get

$$\frac{dM_g}{dt} = S\dot{m} \tag{4.48}$$

Now

$$\begin{aligned} \frac{dM_g}{dt} = \frac{d(\bar{\rho}_g V)}{dt} = V\frac{d\bar{\rho}_g}{dt} + \bar{\rho}_g\frac{dV}{dt} = V\frac{d\bar{\rho}_g}{dt} + \bar{\rho}_g(S\dot{a}), \\ \text{since} \quad \frac{dV}{dt} = \frac{d(4\pi a^3/3)}{dt} = 4\pi a^2\dot{a} = S\dot{a}. \end{aligned} \tag{4.49}$$

so that the final form of the conservation of mass can be written as

$$\boxed{\frac{d\bar{\rho}_g}{dt} = -\frac{3\bar{\rho}_g}{a}\left(\dot{a} - \frac{\dot{m}}{\bar{\rho}_g}\right)} \tag{4.50}$$

4.2.3 Species

Using the divergence theorem and Leibniz's rule the conservation of species can be written as

$$\frac{d}{dt}\int_V \rho_g Y_i dV = \int_S [\rho_g(\vec{v}_b - \vec{v}_g)\cdot\hat{n}]Y_i dS + \int_v \dot{\omega}_i dV \tag{4.51}$$

where we have ignored species diffusion. Using the connection condition for mass, the species equation becomes

$$\frac{d(M_g\bar{Y}_i)}{dt} = \int_S \dot{m}Y_i dS + V\bar{\dot{\omega}}_i. \tag{4.52}$$

The quantaties do not vary along the surface since we are assuming spherical symmetry, so the above reduces to

$$\frac{d(M_g\bar{Y}_i)}{dt} = S\dot{m}Y_i + V\bar{\dot{\omega}}_i \tag{4.53}$$

Using the connection condition for species we get

$$\frac{d(M_g\bar{Y}_i)}{dt} = S\dot{m}Y_{i,c} + V\bar{\dot{\omega}}_i. \tag{4.54}$$

Now

$$\frac{d(M_g\bar{Y}_i)}{dt} = \bar{Y}_i\frac{dM_g}{dt} + M_g\frac{d\bar{Y}_i}{dt} = \bar{Y}_i\dot{m}S + M_g\frac{d\bar{Y}_i}{dt}. \tag{4.55}$$

The final form of the conservation of species can be written as

$$\boxed{\bar{\rho}_g \frac{d\bar{Y}_i}{dt} = \bar{\dot{\omega}}_i + \frac{3}{a}\dot{m}(Y_{i,c} - \bar{Y}_i).} \tag{4.56}$$

4.2.4 Energy

Using the divergence theorem and Leibniz' rule the conservation of energy can be written as

$$\frac{d}{dt}\int_V \rho_g e_{t,g} dV = \int_S [\rho_g(\vec{v}_b - \vec{v}_g)\cdot\hat{n}]e_{t,g}dS - \int_S P_g(\underline{\underline{I}}\cdot\vec{v}_g)\cdot\hat{n}dS. \tag{4.57}$$

Let

$$e_{t,g} = e_g + \frac{1}{2}\vec{v}_g\cdot\vec{v}_g \approx e_g, \tag{4.58}$$

where we have dropped the kinetic energy term due to the low Mach number assumption. We write

$$e_g = e_{g,s} + e_{g,c} = h_g + P_g/\rho_g = h_{g,s} + h_{g,c} + P_g/\rho_g, \tag{4.59}$$

where $e_{g,s} = h_{g,s} + P_g/\rho_g$ is the sensible part of the energy (also called the internal energy), and $e_{g,c} = h_{g,c}$ is the chemical energy. Now note that

$$h_g = \sum Y_i h_{g,i} = \sum Y_i(h_i, s + \Delta h_i^\circ) = h_{g,s} + h_{g,c} \tag{4.60}$$

where $h_{g,s}$ is the sensible enthalpy and $h_{g,c}$ is the chemical enthalpy. Thus, the LHS of Eqn.(4.57) can be written as

$$\begin{aligned}
\frac{d}{dt}\int_V \rho_g e_{t,g} dV &= \frac{d}{dt}\int_V \rho_g e_g dV \\
&= \frac{d}{dt}\int_V \rho_g (e_{g,s} + e_{g,c}) dV \\
&= \frac{d}{dt}\int_V \rho_g e_{g,s} dV + \frac{d}{dt}\int_V \rho_g (\sum \Delta h^\circ_{i,g} Y_i) dV \\
&= \frac{d}{dt}\int_V \rho_g e_{g,s} dV + \sum \Delta h^\circ_{i,g} \frac{d}{dt}\int_V \rho_g Y_i dV \qquad (4.61) \\
&= \frac{d}{dt}\int_V \rho_g e_{g,s} dV + \sum \Delta h^\circ_{i,g} [S\dot{m} Y_{i,c} + V\bar{\dot{\omega}}_i] \\
&= \frac{d}{dt}\int_V \rho_g e_{g,s} dV + V \sum \Delta h^\circ_{i,g} \bar{\dot{\omega}}_i \\
&= \frac{d}{dt}\int_V \rho_g e_{g,s} dV - VQ\Omega
\end{aligned}$$

Here, Q is the heat release and Ω is the reaction source term. We have made use of the conservation of species Eqn.(4.54) to eliminate the time derivative term involving mass fractions. Also, we have taken $\sum \Delta h^\circ_{i,g} = 0$ because we are assuming only a single decomposition gas comes off at the surface; i.e., $Y_{i,c} = Y_c$ and thus $\sum \Delta h^\circ_{i,g} = 0$.

The energy equation now becomes

$$\frac{d}{dt}\int_V \rho_g e_{g,s} dV = \dot{m} e_g S - P_g u_g S + VQ\Omega. \qquad (4.62)$$

Eliminating $e_{g,s}$ in terms of enthalpy, $h_{g,s} = e_{g,s} - P_g/\rho_g$, we get

$$\frac{d}{dt}\int_V \rho_g e_{g,s} dV = \dot{m} h_g S - P_g \dot{a} S + VQ\Omega. \qquad (4.63)$$

Recall that the surface values on the RHS are evaluated at the surface.

Now the enthalpy flux at the surface is not conserved if surface reactions take place, so the flux condition is given by

$$[\dot{h}] = -\dot{m} q S, \qquad (4.64)$$

where q is the surface heat release. Thus,

$$\dot{h}_g = \dot{h}_c + \dot{m}qS, \tag{4.65}$$

i.e.,

$$\dot{m}h_g S = \dot{m}h_c S + \dot{m}qS. \tag{4.66}$$

If we assume $h_c = c_{v,c}T_m$, then the final form of the energy equation can be written as

$$\boxed{\frac{d}{dt}\int_V \rho_g e_{g,s} dV = \dot{m}S(c_{v,c}T_m + q) - P_g \dot{a}S + VQ\Omega} \tag{4.67}$$

The system is closed once an appropriate equation of state is specified.

Kang *et al.*[22] uses a real gas equation of state for the pore gas, the Nobel-Abel equation, defined as

$$P_g = \frac{\rho_g R T_g}{1 - \eta\rho_g}, \tag{4.68}$$

where η is a small parameter. Note that setting $\eta = 0$ we recover the ideal equation of state. In addition, Kang also sets $e_{g,s} = c_v T_g$. Using this relation we get

$$\rho_g e_{g,s} = c_v \rho_g T_g = (c_v/R)P_g(1 - \eta\rho_g) = P_g(1 - \eta\rho_g)/(\gamma - 1), \tag{4.69}$$

so that the volume integral becomes

$$\begin{aligned} \int_V \rho_g e_{g,s} dV &= \frac{1}{\gamma - 1}\int_V P_g(1 - \eta\rho_g)dV \\ &= \frac{1}{\gamma - 1}P_g \int_V (1 - \eta\rho_g)dV = \frac{1}{\gamma - 1}P_g(V - \eta M_g). \end{aligned} \tag{4.70}$$

The time derivative of the volume integral now becomes

$$\begin{aligned} \frac{dP_g}{dt}\int_V \rho_g e_{g,s} dV &= \frac{1}{\gamma - 1}\frac{d}{dt}[P_g V - \eta M_g P_g] \\ &= \frac{V(1 - \eta\bar{\rho}_g)}{\gamma - 1}\frac{dP_g}{dt} + \frac{P_g S\dot{a}}{\gamma - 1} - \frac{\eta P_g S\dot{m}}{\gamma - 1}, \end{aligned} \tag{4.71}$$

so that the final form of the energy equation can be written as

$$\frac{dP_g}{dt} = \frac{1}{1-\eta\bar{\rho}_g}\left\{3/a[-P_g\dot{a} + \eta P_g\dot{m} + (\gamma-1)(-P_g\dot{a} + \dot{m}c_{v,c}T_m + \dot{m}q)]\right.$$
$$\left. + (\gamma-1)Q\Omega\right\}. \tag{4.72}$$

4.3 Summary of Equations

We have derived all the equations needed to perform the calculation. Computationally, we separate the process into two steps: (i) pre-melting process, where no chemical reactions are taken into consideration, and the entire gas-phase effects are neglected which make the equations to be further simplified; (ii) post-melting process, in this part a one-step chemical reaction is added to the system; and by averaging the density, mass fraction, temperature and pressure of the gas-phase the system then becomes a set of ODEs.

4.3.1 Pre-melting Process

The governing equations present here only show the change of inner radius and the condensed-phase temperature at the interface

$$\begin{aligned}
\frac{da}{dt} &= \frac{a}{4\mu_c(1-\phi)}\left\{P_g - P_s + 2\bar{Y}\ln\left(\frac{b}{a}\right)\right\},\\
\frac{dT_c}{dt} &= \frac{1}{\rho_c c_{v,c}}\left\{\frac{12\mu_c a^4\dot{a}^2}{[a^3+(r_0^3-a_0^3)]^2} + \frac{2\bar{Y}a^2|\dot{a}|}{a^3+(r_0^3-a_0^3)}\right\},\\
\frac{d\rho_g}{dt} &= -3\rho_g\frac{\dot{a}}{a}.
\end{aligned} \tag{4.73}$$

4.3.2 Post-melting Process

The final set of equations for the post-melting processes is

$$\begin{aligned}
\frac{da}{dt} &= \frac{\dot{m}}{\rho_c} - \frac{a}{4\mu_c}\left[P_s - P_g - \dot{m}^2\left(\frac{1}{\rho_g} - \frac{1}{\rho_c}\right) - 2\overline{Y}\ln\left(\frac{b_m}{a}\right)\right], \\
\frac{d\rho_g}{dt} &= -\frac{3\rho_g}{a}\left(\dot{a} - \frac{\dot{m}}{\rho_g}\right), \\
\frac{dY}{dt} &= \frac{3\dot{m}}{a\rho_g}(Y_c - Y) - \frac{\Omega}{\rho_g}, \\
\frac{dP_g}{dt} &= \frac{1}{1-\eta\bar{\rho}_g}\left\{3/a[-P_g\dot{a} + \eta P_g\dot{m} + (\gamma-1)(-P_g\dot{a} + \dot{m}c_{v,c}T_m + \dot{m}q)]\right. \\
&\quad \left. +(\gamma-1)Q\Omega\right\}, \\
\Omega &= D_a Y P_g^n \exp(-E_g/R_u T), \\
T_g &= \frac{P_g(1-\eta\rho_g)}{\rho_g R_g}.
\end{aligned} \tag{4.74}$$

The parameters without a subscript are condensed phase parameters; the gas phase quantities all have a subscript g.

4.4 Numerical Solution

The governing equations are solved numerically with the parameters of the condensed phase chosen to represent RDX and HMX. The parameters are given in Table 3.1, and the initial conditions are given in Table 3.2.

Table 4.1: Initial Conditions

Parameter	**Value**
a_0 [m]	5.0×10^{-6}
$\dot{a}_0$ [m/s]	0.0
ϕ_0	0.05
$P_{g,0}$ [Pa]	10^5
$T_{g,0}$ [K]	300.0
$T_{c,0}$ [K]	300.0
Y_0	1.0

Table 4.2: Parameters of RDX and HMX

Parameter	**Unit**	**RDX**	**HMX**
$c_{v,c}$	[J/kg-K]	$1,465.0$	$1,031.0$
D_a	$[s^{1.44}/(m^{1.78} \cdot kg^{0.22})]$	$10,798.0$	$19,300.0$
E_g/R	[K]	$16,400.0$	$22,000.0$
n		1.22	1.22
T_m	[K]	558.0	548.0
ρ_c	$[kg/m^3]$	$1,806.0$	$1,905.0$
μ_c	$[kg/(s \cdot m)]$	50.0	65.0
β	[K/Pa]	2.0×10^{-7}	1.8×10^{-7}
$\overline{Y}_0$	$[N/m^2]$	1.1×10^8	2.0×10^8

4.4.1 Numerical Solution with First Order Interface Equation

Eqn.(4.73, 4.74) are used in this section to calculate the evolution of the interface.

Numerical Solution prior to Melting

Before condensed-phase temperature at the interface reaches its post-shock melting temperature, we use Eqn.(4.73) to calculate the change of inner radius, interface temperature and gas-phase density. We neglect the heat conduction between condensed phase and gas phase because of the assumption that gas-phase temperature always stays the same as the condensed-phase temperature at the interface. Once the density and temperature are obtained, we can use the Nobel-Abel equation to determine the gas pressure. The results are shown as follows.

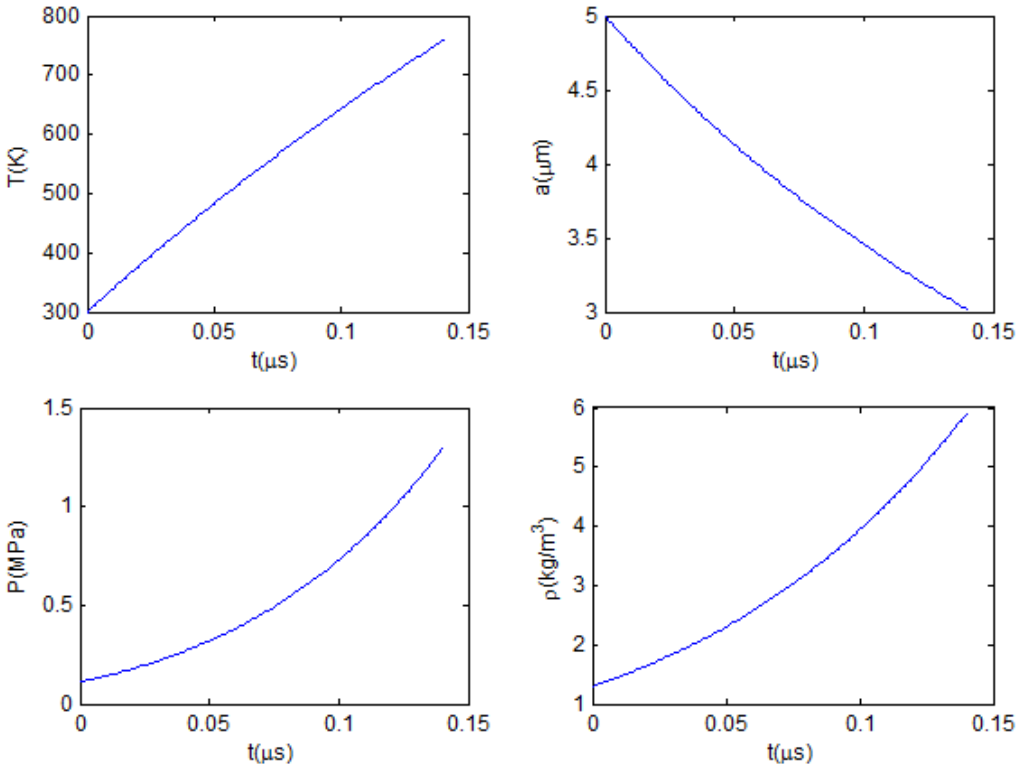

Figure 4.1: Pre-melting solution (RDX)

These results show that during the pre-melting process, the pore collapses under the effect of shock pressure. It causes the condensed-phase interface temperature increases and finally makes it to reach the melting temperature, $T_{\text{melt}} = 758$ K, at $t_{\text{melt}} = 0.131\mu$s. During this process, the gas-phase pressure and density also increase due to the reduction of pore size. However, the change in this stage is not significant since no chemical reaction has yet been introduced. The result of pre-melting solution for HMX is also obtained and is shown in the following figures.

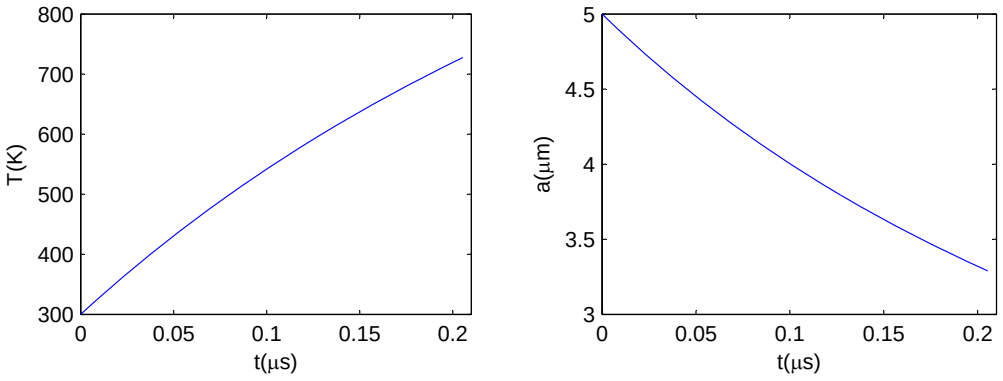

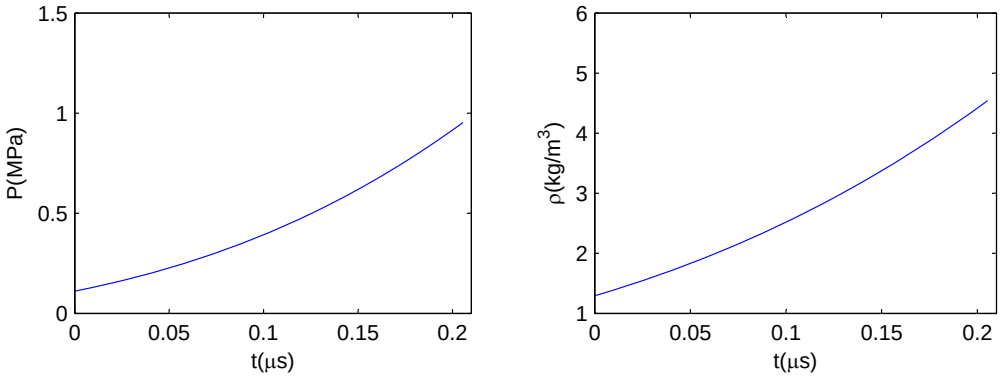

Figure 4.2: Pre-melting solution (HMX)

These results show similar trends in the variations of interface temperature, pore radius, gas-phase pressure, and gas-phase density with respect to time as they are in the RDX case. However, a larger value in the material viscosity and yield stress causes it to take more time, $t_{\text{melt}} = 0.205\mu$s, for the interface to reach a even lower melting temperature, $T_{\text{melt}} = 728$K. In both cases, we observe that the change of interface temperature in this stage almost keeps a linear relationship with time.

Numerical Solution after Melting

As the interface reaches the melting temperature, sublimation occurs at the interface and chemical reaction is turned on inside the void. Therefore Eqn(4.74) are used to simulate the process from this point on.

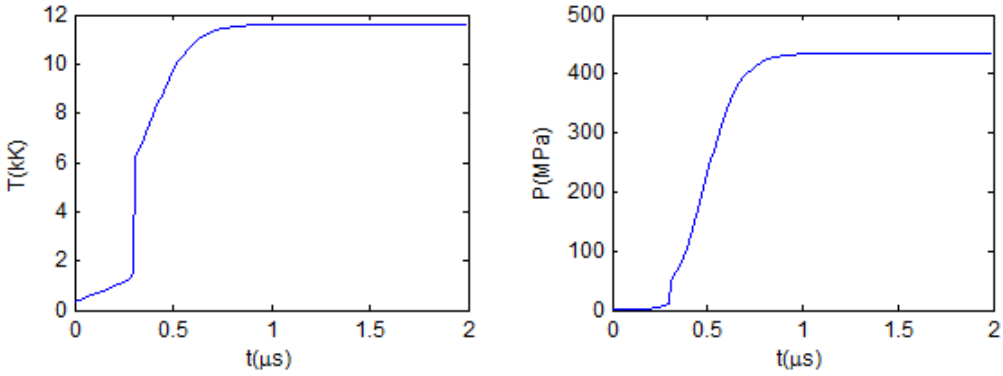

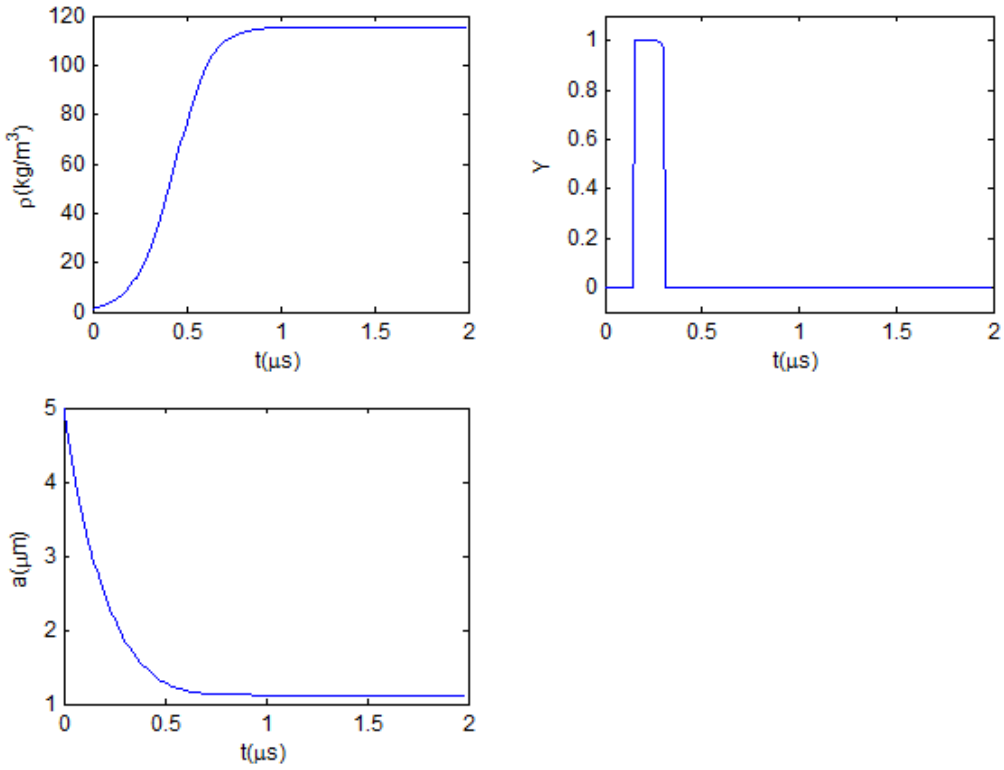

Figure 4.3: Numerical solution with first order interface equation (RDX)

Figure (4.3) shows pore collapse results for RDX with the initial condition stated in Table 4.1. The figures show abrupt changes in gas temperature and pressure. These changes include not only those seen obviously around $t = 0.3\mu s$ but also the less significant ones occurred immediately after the pre-melting stage. When condensed-phase interface reaches melting temperature, sublimated energetic material enters into pore to react, causing gas-phase density, temperature and pressure to increase as a whole. However, the changes at this moment are not large enough to offset the effects of shock pressure. Thus, the pore keeps collapsing until the point it reaches a steady state or expands. However, in this result we does not observe the phenomenon of pore expansion. This is because that the first-order interface equation fails to consider the change of direction in interface velocity during the post-melting process, thus pore expansion may not be recorded in the results. This problem will be resolved immediately in the following model. The following figures show the pore collapse results for HMX under the same condition.

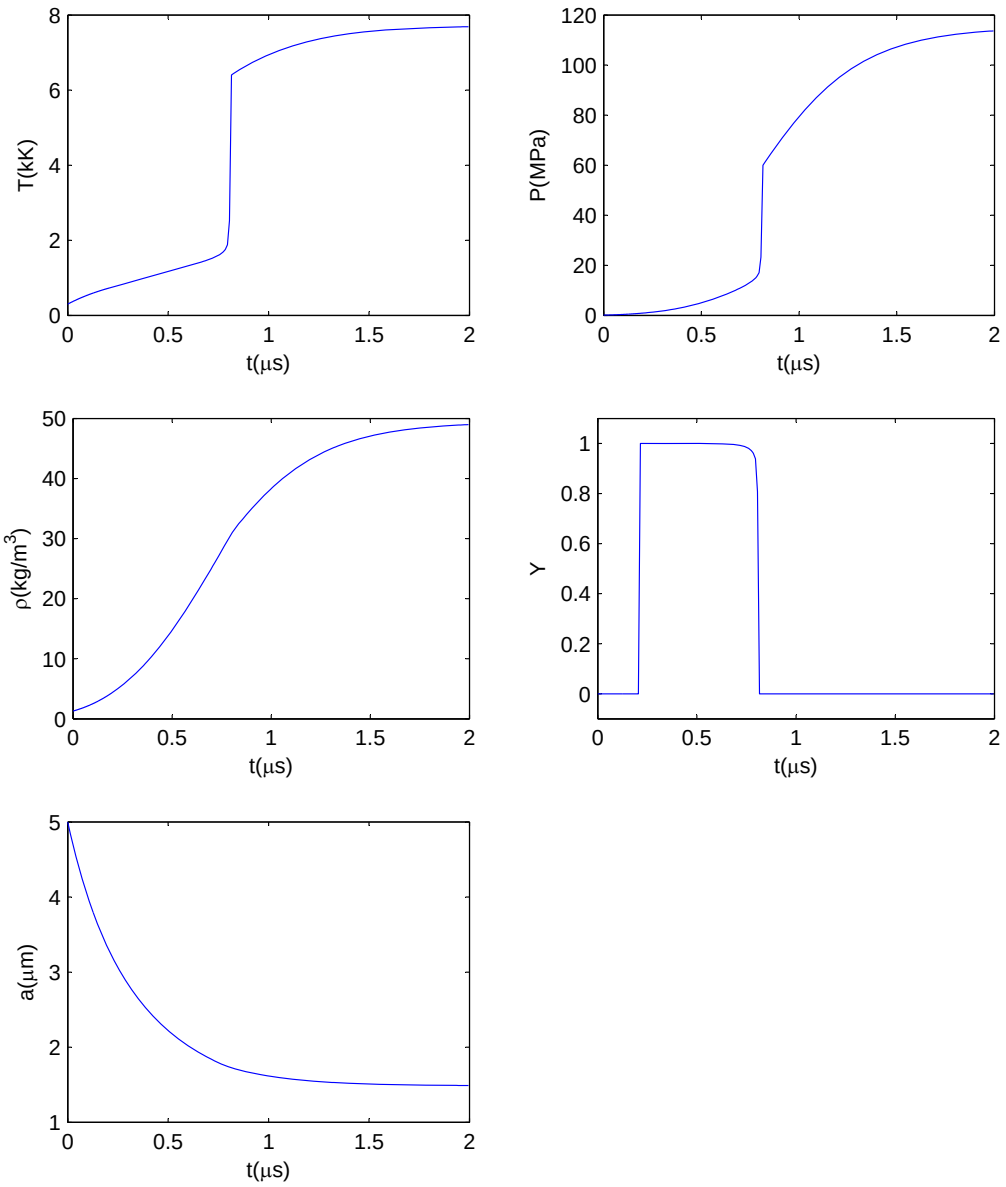

Figure 4.4: Numerical solution with first order interface equation (HMX)

Again, the results are of the similar type as they are for RDX. Although this model fails to take the change in direction of the interface velocity into consideration, it successfully captures the import facts, such as sublimation and reaction, in the post-melting process. Therefore, we will continue working on this model, but will replace the interface velocity equation to solve the problem.

4.4.2 Numerical Solution with Second Order Interface Equation

In this part, the interface equation is switched to a second order PDE involving ξ, which is related with a and b through the following equations

$$\frac{d\xi}{dt} = \frac{1}{a\rho_c(1-\phi^{1/3})}\left\{P_g - P_s - 4\mu_c\frac{\xi}{a}(1-\phi) - \dot{m}^2\left(\frac{1}{\rho_c}-\frac{1}{\rho_g}\right) - \right.$$
$$\left. - 2\bar{Y}\mathrm{sgn}(\xi)ln\left(\frac{b}{a}\right) - 2\rho_c\xi\left(\xi+\frac{\dot{m}}{\rho_c}\right)\left(1-\phi^{1/3}\right) + \frac{\rho_c}{2}\xi^2\left(1-\phi^{4/3}\right)\right\}, \tag{4.75}$$

$$\frac{da}{dt} = \xi + \frac{\dot{m}}{\rho_c}, \tag{4.76}$$

$$\frac{db}{dt} = \left(\frac{a}{b}\right)^2\xi. \tag{4.77}$$

We no longer separate the calculation into pre-melting and post-melting because the 'sgn' function can automatically take the velocity direction into consideration. With this new model, pore collapse results for RDX and HMX are obtained as follows.

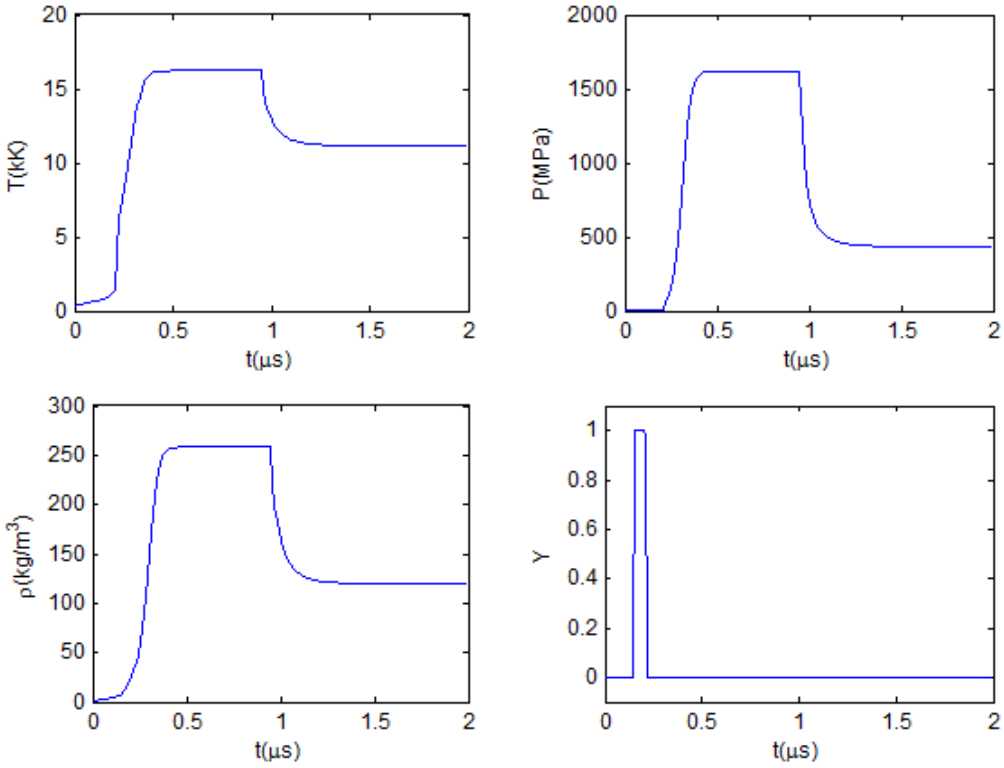

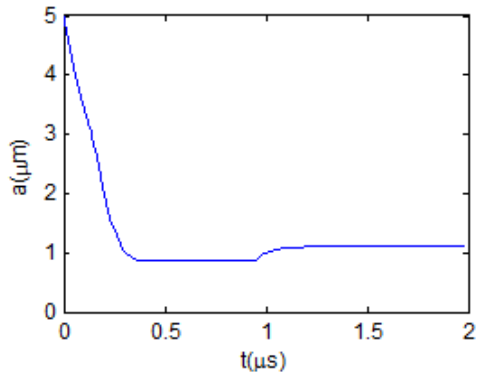

Figure 4.5: Numerical solution with second order interface equation (RDX)

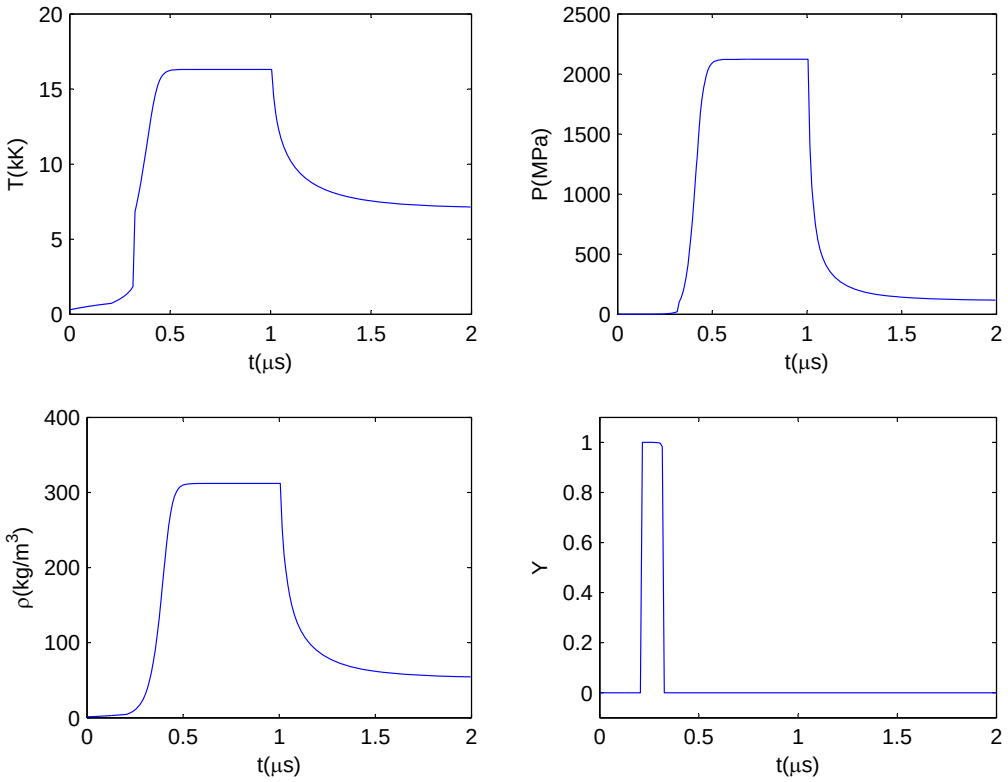

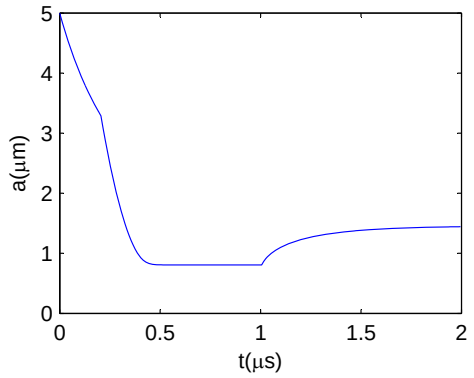

Figure 4.6: Numerical solution with second order interface equation (HMX)

The result shows that the time of the pore collapse is of the same order as the one we obtained from previous numerical solutions using first order interface equation. It reveals that pore actually expands at certain time. However, from the figures we observe that the pore goes through a steady state before it starts to expand; and the maximum gas-phase temperature is too high. This is because that in our previous derivation, we neglected the effect of heat conduction between gas and solid phases. However, this assumption may not hold if the gas phase temperature becomes much higher than the solid phase when the reaction is turned on. Our second numerical model will take the heat conduction effect into consideration. Detailed information will be presented as the discussion expands.

4.5 Discussion

Now that the numerical model for hot spot generation has been established, we will run several cases to test the impact of initial conditions to its formation. Considering the similar properties of RDX and HMX, we will focus our study on RDX in the following analysis.

4.5.1 Initial Condition Analysis

First, we keep the parameters of the physical model constant, $a_0 = 5$ μm, and change the post shock pressure from 1GPa to 9Gpa. Define the induction time to be the moment when a burning pore reaches its minimum radius. This

parameter contains the material response as well as the chemical reaction information[1].

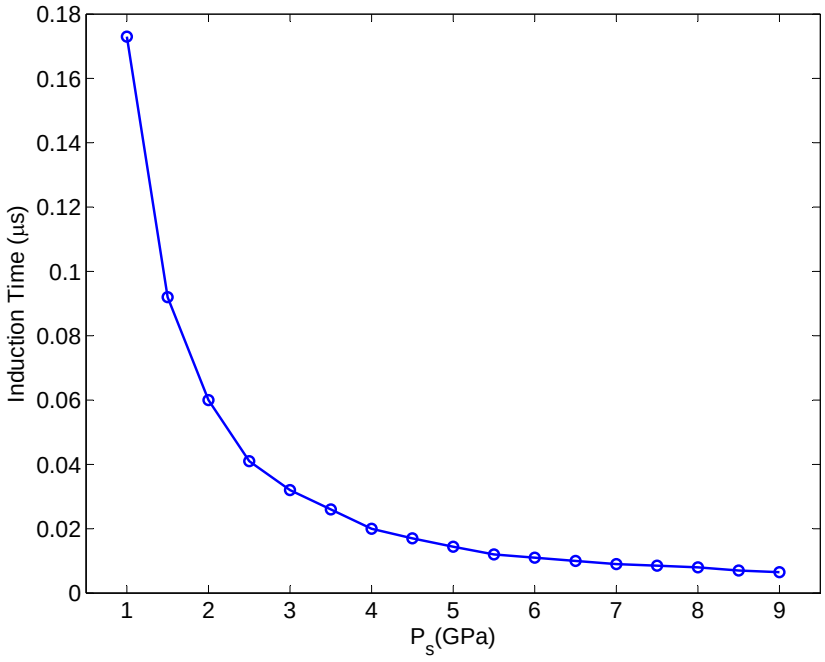

Figure 4.7: Variation of induction time, τ

Figure(4.7) shows that as the shock pressure increases the induction time decreases. This decreasing trend is more significant for $P_s < 5$ GPa, but the trend is more general when the pressure is much larger. This is understandable, since the pore collapse faster under high shock pressure. The visco-plastic effect is more significant when the condensed-phase material is moving at a larger speed, which makes the interface to reach melting temperature soon and turns on the chemical reaction to prevent further collapse.

To obtain a through understanding of the impact of initial condition to the numerical results of our model, we calculate the induction time for the model with varying pore radius between 0.5 to 5.0 μm at different viscosity, $\phi \in [0.005, 0.05]$. The result is presented in an error plot shown below.

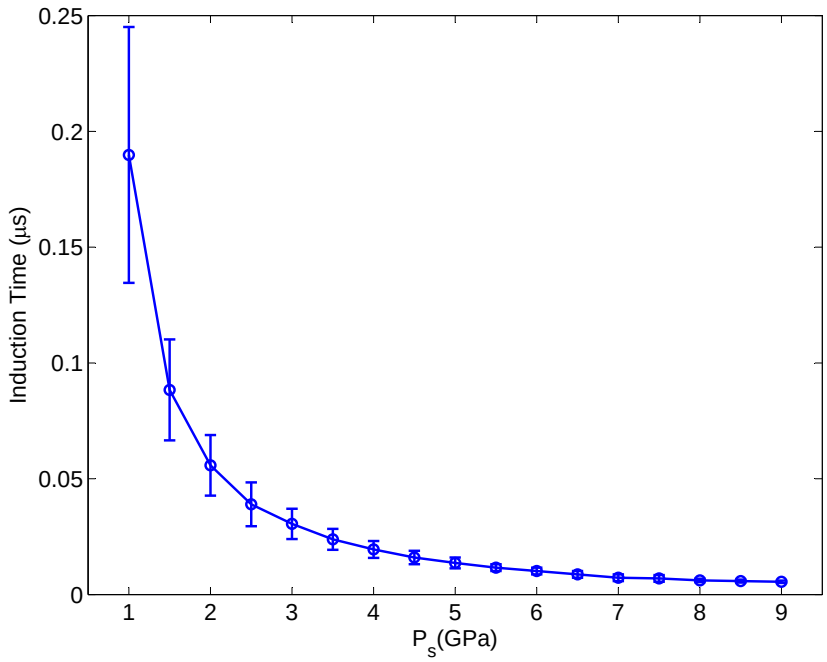

Figure 4.8: Induction time τ as a function of shock pressure P_s for $\phi \in [0.005, 0.05]$ and $a_0 \in [0.5, 5.0]$ microns. The curve is the mean through the data, and the error bars represent the largest and smallest set of values at each shock pressure.

4.5.2 The Influence of $\dot{a}$ on Numerical Solution

Kang[22] and Massoni[17] used the assumption, $\dot{a}_0 = 0$, as the initial interface velocity. However, we can use the first and second order interface equations to obtain a more reasonable starting value for $\dot{a}$.

Approximation solution:

$$\frac{a}{a_0} = \exp\left[-t\left\{\frac{P_s}{4\,\mu_c} - \frac{\bar{Y}}{2\,\mu}\ln\left(\frac{b_0}{a_0}\right)\right\}\right] = \exp[-\nu\,t]$$

$$a(t) = a0 \times \exp[-5.7445\text{E}6\,t] \tag{4.78}$$

First order ode:

$$\frac{d\,a}{d\,t} = \frac{a}{4\mu_c(1-\phi)}\left\{-P_s + 2\,\bar{Y}\ln\left(\frac{b}{a}\right)\right\} \tag{4.79}$$

Second order ode:

$$\frac{d\xi}{dt} = \frac{1}{a\rho_c(1-\phi^{1/3})}\left\{P_g - P_s - 4\mu_c\frac{\xi}{a}(1-\phi) - 2\bar{Y}sgn(\xi)ln\left(\frac{b}{a}\right) - 2\rho_c\xi^2\left(1-\phi^{1/3}\right) + \frac{\rho_c}{2}\xi^2\left(1-\phi^{4/3}\right)\right\} \quad (4.80)$$

We can use these these equations to calculate the initial interface velocity. And the following figures present the difference between the change of inner radius a under different $\dot{a}_0$ during the pre-melting process:

- First order ODE solution, Eqn.(4.79);
- Simplified analytic solution, Eqn.(4.78);
- Second order ODE with $a(0) = a_0$ with $\dot{a}(0) = 0$;
- Second order ODE with $a(0) = a_0$ with $\dot{a}(0)$ obtained by Eqn.(4.79);
- Second order ODE with $a(0) = a_0$ with $\dot{a}(0)$ obtained by Eqn.(4.78).

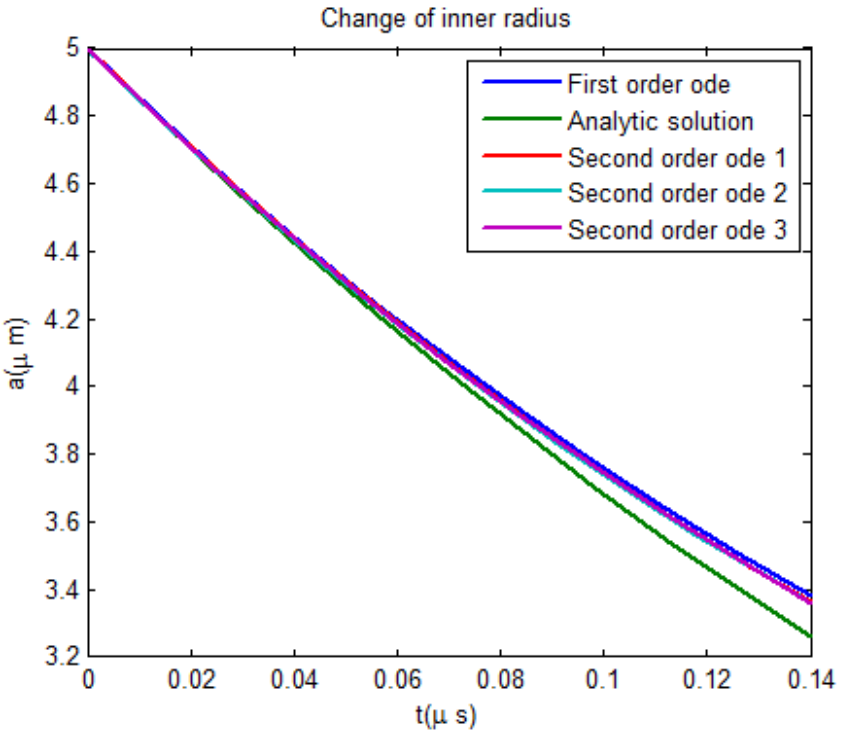

Figure 4.9: Impact of initial interface velocity

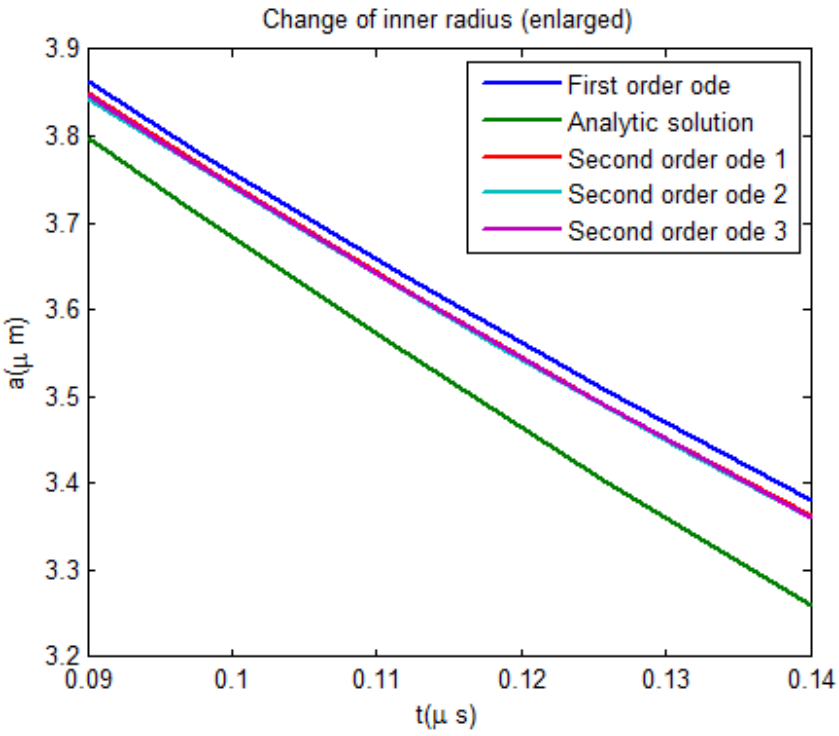

Figure 4.10: Impact of initial interface velocity (enlarged)

From the figures, we can see that the difference between these $\dot{a}_0$ is trivial except for the analytic one, which has been greatly simplified. Thus, we will continue to use the assumption $\dot{a}_0 = 0$ in our following calculations so that the solution is comparable with other work.

CHAPTER 5

FULLY DISCRETE MODEL

In the previous model we averaged the gas-phase governing equations over the pore to get a set of ordinary differential equations. This model is similar to Kang's[22] model except that our scaling discussion made some further simplification, while it retained reasonable results. In this chapter we will justify the validity the spatial averaging technique by solving the partial equations directly.

The physics of a pore collapse is complex. At relatively high shock pressures, the early stages of pore collapse is dominated by viscoplastic heating, raising the condensed-phase temperature near the pore interface. The material softens, and the pore begins to collapse. Once the interface temperature reaches the melting temperature, the condensate is converted to gas, and there is a mass flux of gases into the pore. These gases are reactive, and the rising temperature and pressure in the pore eventually lead to ignition. Subsequent events lead to large gas-phase pressures, which can balance the applied shock pressure and the collapse is abruptly terminated. Further increases in the gas-phase pressure leads to a reversal of the pore interface, which now begins to expand. While the process of pore collapse and reversal takes place, thermal energy in the pore is transferred to the condensate, raising the condensate temperature near the interface above the ignition point, leading to reaction in the condensate.

5.1 Governing Equations

5.1.1 Gas Phase

In the pore region ($0 < r < a(t)$) the appropriate low Mach number equations for a reactive gas are given by

$$\frac{\partial \rho}{\partial t} + \frac{1}{r^2}\frac{\partial}{\partial r}(r^2 \rho u) = 0, \tag{5.1}$$

$$\rho c_p \left[\frac{\partial T}{\partial t} + u\frac{\partial T}{\partial r}\right] - \frac{d\,P}{d\,t} = \frac{\lambda_g}{r^2}\frac{\partial}{\partial r}\left(r^2 \frac{\partial T}{\partial r}\right) + Q_g \Omega_g, \tag{5.2}$$

$$\rho \left[\frac{\partial Y}{\partial t} + u\frac{\partial Y}{\partial r}\right] = \frac{\rho D}{r^2}\frac{\partial}{\partial r}\left(r^2 \frac{\partial Y}{\partial r}\right) - \Omega_g. \tag{5.3}$$

We do not solve the momentum equation because this only determines the hydrodynamic pressure, which is of order Mach number squared. The Nobel-Abel equation of state is given by

$$P = \frac{\rho R_g T}{1 - \eta\rho}. \tag{5.4}$$

Here, $P = P(t)$ is a function time. The global reaction rate Ω_g is given by

$$\Omega_g = A_g Y P^n \exp(-E_g/R_u T). \tag{5.5}$$

In the low Mach number limit the continuity equation is a constraint on the velocity field. Starting with the continuity equation, and using the gas law and energy equation to eliminate time derivatives of the density and temperature, an equation for the gas-phase velocity can be derived, yielding

$$\frac{1 - \gamma\eta\rho}{\gamma}\frac{dP}{dt} + \frac{P}{r^2}\frac{\partial}{\partial r}(r^2 u) = \frac{\gamma - 1}{\gamma}\left[\frac{\lambda_g}{r^2}\frac{\partial}{\partial r}\left(r^2 \frac{\partial T}{\partial r}\right) + Q_g \Omega_g\right]. \tag{5.6}$$

The pressure is updated by integrating Eqn.(5.6) over the pore volume. Multiplying by r^2 and then integrating over the pore radius, we get

$$\frac{dP}{dt} = \frac{3}{a(1 - \gamma\eta\bar{\rho})}\left\{-\gamma P(\dot{a} - \dot{m}/\rho_g|_{a^-}) + (\gamma - 1)\lambda_g \frac{\partial T}{\partial r}\right\} + \frac{\gamma - 1}{1 - \gamma\eta\bar{\rho}} Q_g \overline{\Omega}_g, \tag{5.7}$$

where

$$\bar{\rho} = \frac{\int_0^a r^2 \rho dr}{a^3/3}, \qquad \overline{\Omega}_g = \frac{\int_0^a r^2 \Omega_g dr}{a^3/3}. \tag{5.8}$$

The density is found from the equation of state

$$\rho_g = \frac{P}{R_g T + \eta P}. \tag{5.9}$$

To summarize, in the pore region ($0 < r < a(t)$) we solve Eqn.(5.2 - 5.3) for the temperature T_g and the species Y_g, respectively; Eqn.(5.6) for the velocity u_g; Eqn.(5.7) for the pressure P_g; and Eqn.(5.9) for the density ρ_g.

5.1.2 Condensed Phase

In the condensed phase ($a(t) < r < b(t)$) the incompressible equations are given by

$$\rho_c c_c \left[\frac{\partial T}{\partial t} + u_c \frac{\partial T}{\partial r} \right] = \frac{\lambda_c}{r^2} \frac{\partial}{\partial r} \left(r^2 \frac{\partial T}{\partial r} \right) + \Phi_c. \tag{5.10}$$

Here,

$$\Phi_c = 12 \mu_c \frac{u_c^2}{r^2} + 2 \overline{Y} \frac{|u_c|}{r}, \tag{5.11}$$

is the viscous dissipation term.

The velocity in the condensed phase is given by

$$u_c = \left(\frac{a}{r} \right)^2 (\dot{a} - \dot{m}/\rho_c). \tag{5.12}$$

The mass flux is given by

$$\dot{m} = \begin{cases} 0 & \text{for } T_c < T_{melt} \\ \\ \rho_c S r_b & \text{for } T_c \geq T_{melt} \end{cases} \tag{5.13}$$

where $S = 4\pi a^2$ is the surface area of the pore and r_b the burning rate defined by the pyrolysis law

$$r_b = A_b \exp(-E_b / R_u T_s) \tag{5.14}$$

with T_s the surface temperature. The value of A_b is calibrated to yield time scales roughly on the same order as that of King.

Note that the mass flux is not turned on numerically until the interface temperature reaches the melting temperature. Also, the viscosity is less in the melt layer than in the condensate, and to account for this we use Kang's relation

$$\mu_c = \begin{cases} \mu_{c,0} \exp\left[\alpha_\mu P_s \frac{T_0}{T_c}\right], & \text{for } T_c < T_{melt} \\ \\ \mu_{c,0} \exp\left[\frac{E_\mu}{R_\mu}\left(\frac{1}{T_c} - \frac{1}{T_{melt}}\right) + \alpha_\mu P_s \frac{T_0}{T_c}\right], & \text{for } T_c \geq T_{melt} \end{cases} \tag{5.15}$$

with T_c the condensed-phase temperature. We further note that the yield strength is zero in the melt layer, so that

$$\overline{Y} = \begin{cases} \overline{Y}_0 \frac{T_{melt} - T_c}{T_{melt} - T_0} & \text{for } T_c \leq T_{melt} \\ \\ 0 & \text{for } T_c \geq T_{melt} \end{cases} \tag{5.16}$$

The viscous dissipation term then becomes

$$\Phi_c = \begin{cases} 12\mu_c \frac{u_c^2}{r^2} + 2\overline{Y}\frac{|u_c|}{r} & \text{for } T_c < T_{melt} \\ \\ 12\mu_c \frac{u_c^2}{r^2} & \text{for } T_c \geq T_{melt} \end{cases} \tag{5.17}$$

5.1.3 Interface Motion

A differential equation for the interface motion has been previously derived, and is given by

$$\begin{aligned} \frac{d\zeta}{dt} = \frac{1}{a\rho_c(1-\phi^{1/3})} \Bigg\{ & P_g - P_s - p_v + P_y - \dot{m}^2 \left(\frac{1}{\rho_c} - \frac{1}{\rho_g}\right) \\ & -2\rho_c\zeta \left(\zeta + \frac{\dot{m}}{\rho_c}\right)(1-\phi^{1/3}) + \frac{\rho_c}{2}\zeta^2(1-\phi 4/3) \Bigg\}, \end{aligned} \tag{5.18}$$

where

$$p_v = 12a^2\zeta \int_a^b \frac{\mu_c}{r^4} dr, \quad p_y = 2\text{sgn}(\zeta) \int_a^b \frac{\overline{Y}}{r} dr, \tag{5.19}$$

and

$$\zeta(t) = \dot{a} - \frac{\dot{m}}{\rho_c}, \quad \phi = \left(\frac{a}{b}\right)^3. \tag{5.20}$$

This is a second-order ODE for $a(t)$. To integrate, the initial conditions $a(0) = a_0$ and the value of $\dot{a}(0)$ are needed; the initial velocity is one that is not readily available. We follow Kang and set $\dot{a}(0) = 0$. The equation for b is given by

$$\frac{d}{dt}(b^3) = \frac{d}{dt}(a^3), \tag{5.21}$$

with initial condition $b(0) = a(0)/\phi^{1/3}$.

5.1.4 Boundary and Initial Condition

Boundary conditions at $r = 0$ are given by

$$u = 0, \quad \frac{\partial T}{\partial r} = 0, \quad \frac{\partial Y}{\partial r} = 0. \tag{5.22}$$

Initial conditions in the gas phase $0 < r < a$ are

$$P = P_0, \quad T = T_0, \quad Y = 1. \tag{5.23}$$

We take $P_0 = 1$ atm and $T_0 = 300$ K. The initial condition for the temperature in the condensed phase is given by

$$T_c = T_s, \tag{5.24}$$

where T_s is the shocked temperature in the solid corresponding to the shock pressure P_s. The shocked temperature is lower than the melting temperature, defined by

$$T_{melt} = T_{melt,0} + \beta P_s. \tag{5.25}$$

The constants $T_{melt,0}$ and β are known for a given material.

5.1.5 Connection Conditions

The connection conditions across the condensed-gas interface are given by

$$\begin{aligned} [\rho(u-\dot{a})] &= -\dot{m}, \\ [T] &= 0, \\ [cT]\dot{m} &= [\lambda \hat{n}\cdot\nabla T] + q\dot{m}, \\ [\rho D \hat{n}\cdot\nabla Y] &= \dot{m}[Y], \end{aligned} \tag{5.26}$$

where q is the heat release at the interface. The normal $\hat{n}$ is pointing towards the gas so that $\hat{n} = -\hat{e}_r$. The jump in the mass flux can be written as

$$\rho_g(u_g - \dot{a}) = \rho_c(u_c - \dot{a}) = -\dot{m}. \tag{5.27}$$

The jump in the energy can be written as

$$(c_p - c_c)T_s\dot{m} = -\lambda_g \left.\frac{\partial T}{\partial r}\right|_g + \lambda_c \left.\frac{\partial T}{\partial r}\right|_c + q\dot{m}. \tag{5.28}$$

The jump in the species can be written as

$$-\rho D \left.\frac{\partial Y}{\partial r}\right|_g = \dot{m}(Y_g - 1). \tag{5.29}$$

In what follows we take $c_p = c_v$.

5.2 Transformations

Since the interface moves in time, we introduce transformations such that in the computational domain the interface is fixed.

5.2.1 Gas-phase Transformation

In the gas phase $0 < r < a(t)$ we define

$$\xi_1 = \frac{r}{a}, \quad 0 < \xi_1 < 1. \tag{5.30}$$

Then

$$\frac{\partial}{\partial t} = \frac{\partial}{\partial t} - \frac{\dot{a}\xi_1}{a}\frac{\partial}{\partial \xi_1}, \quad \frac{\partial}{\partial r} = \frac{1}{a}\frac{\partial}{\partial \xi_1}. \tag{5.31}$$

The gas-phase equations in the transformed plane are

$$\rho c_p \left[\frac{\partial T}{\partial t} - \frac{\dot{a}\xi_1}{a}\frac{\partial T}{\partial \xi_1} + \frac{u}{a}\frac{\partial T}{\partial \xi_1}\right] - \frac{dP}{dt} = \frac{\lambda_g}{a^2}\left[\frac{\partial^2 T}{\partial \xi_1^2} + \frac{2}{\xi_1}\frac{\partial T}{\partial \xi_1}\right] + Q_g \Omega_g, \tag{5.32}$$

$$\rho \left[\frac{\partial Y}{\partial t} - \frac{\dot{a}\xi_1}{a}\frac{\partial Y}{\partial \xi_1} + \frac{u}{a}\frac{\partial Y}{\partial \xi_1}\right] = \frac{\rho D}{a^2}\left[\frac{\partial^2 Y}{\partial \xi_1^2} + \frac{2}{\xi_1}\frac{\partial Y}{\partial \xi_1}\right] - \Omega_g, \tag{5.33}$$

$$\frac{1-\gamma\eta\rho}{\gamma}\frac{dP}{dt} + \frac{P}{a}\left(\frac{\partial u}{\partial \xi_1} + \frac{2u}{\xi_1}\right) = \frac{\gamma - 1}{\gamma}\left[\frac{\lambda_g}{a^2}\left(\frac{\partial^2 T}{\partial \xi_1^2} + \frac{2}{\xi_1}\frac{\partial T}{\partial \xi_1}\right) + Q_g \Omega_g\right] \tag{5.34}$$

and

$$\rho = \frac{P}{R_g T + \eta P} \tag{5.35}$$

The global pressure equation becomes

$$\begin{aligned}\frac{dP}{dt} = {} & \frac{3}{a(1-\gamma\eta\bar{\rho})}\left\{-\gamma P(\dot{a} - \dot{m}/\rho_g|_{a^-}) + (\gamma - 1)\frac{\lambda_g}{a}\left.\frac{\partial T}{\partial \xi_1}\right|_{a^-}\right\} \\ & + \frac{\gamma - 1}{1-\gamma\eta\bar{\rho}} Q_g \overline{\Omega}_g,\end{aligned} \tag{5.36}$$

where

$$\bar{\rho} = 3\int_0^1 \xi_1^2 \rho_g \, d\xi_1, \tag{5.37}$$

$$\bar{\Omega}_g = 3\int_0^1 \xi_1^2 \Omega_g \, d\xi_1. \tag{5.38}$$

5.2.2 Condensed Phase Transformation

In the condensed phase $a(t) < r < b(t)$ we define

$$\xi_2 = \frac{r - 2a + b}{b - a}, \quad 1 < \xi_2 < 2, \tag{5.39}$$

i.e.,

$$r = (b - a)\xi_2 + 2a - b. \tag{5.40}$$

Then

$$\frac{\partial}{\partial t} = \frac{\partial}{\partial t} + \frac{d\xi_2}{dt}\frac{\partial}{\partial \xi_2}, \tag{5.41}$$

$$\frac{\partial}{\partial r} = \frac{1}{b-a}\frac{\partial}{\partial \xi_2}, \tag{5.42}$$

where

$$\frac{d\xi_2}{dt} = \frac{1}{b-a}\left[\dot{b}(1-\xi_2) + \dot{a}(\xi_2 - 2)\right]. \tag{5.43}$$

The condensed-phase equations in the transformed plane are

$$\rho_c c_c \left[\frac{\partial T}{\partial t} + \left(\frac{d\xi_2}{dt} + \frac{u}{b-a}\right)\frac{\partial T}{\partial \xi_2}\right] = \frac{\lambda_c}{(b-a)^2}\left[\frac{\partial^2 T}{\partial \xi_2^2} + \frac{2(b-a)}{(b-a)\xi_2 + 2a - b}\frac{\partial T}{\partial \xi_2}\right] + \Phi_c, \tag{5.44}$$

$$u_c = \left(\frac{a}{(b-a)\xi_2 + 2a - b}\right)^2 (\dot{a} - \dot{m}/\rho_c). \tag{5.45}$$

5.3 Results and Discussion

The governing equations together with the initial and interface conditions for the discrete hot spot model are solved numerically in two cases. Fourth-order Runge-Kutta scheme and second-order central difference scheme are chosen to represent the temporal and spatial derivatives respectively. The energetic material surrounding the pore is RDX and HMX in each case. The same initial conditions are selected for these calculations as they are in the previous chapter, i.e. Table (5.1). The material properties and constants are summarized in Table (5.2). These parameters are chosen from Kang[22], Doolan[1] and Hamate's[24] papers.

Table 5.1: Initial Conditions

Parameter	**Value**
a_0 [m]	5.0×10^{-6}
$\dot{a}_0$ [m/s]	0.0
ϕ_0	0.05
$P_{g,0}$ [Pa]	10^5
P_s [Pa]	1.0×10^9
$T_{g,0}$ [K]	300.0
$T_{c,0}$ [K]	300.0
Y_0	1.0

Table 5.2: Parameters of RDX and HMX

Parameter	**Unit**	**RDX**	**HMX**
A_g	$[s^{1.44}/(m^{1.78} \cdot kg^{0.22})]$	10798.0	10798.0
E_g	[J/kmol]	1.36×10^8	1.36×10^8
R_g	[J/kg *cdot* K]	287.04	287.04
Q_g	[J/kg]	1.1×10^6	1.1×10^6
c_p	$[J/(kg \cdot K)]$	1465.0	1031.0
n		1.22	1.22
λ_g	$[W/(m \cdot K)]$	0.0833	0.0833
η	$[m^3/kg]$	0.001	0.001
A_b	[1/s]	5.0×10^{15}	5.0×10^{15}
E_b	[J/mol]	1.93×10^8	2.206×10^8
c_c	$[J/(kg \cdot K)]$	1465.0	1031.0
λ_c	$[W/(m \cdot K)]$	0.2093	0.40585
$\overline{Y}_0$	$[N/m^2]$	1.1×10^8	2.0×10^8
ρ_c	$[kg/m^3]$	1806.0	1905.0
μ_c	$[kg/(s \cdot m)]$	50.0	65.0
β	[K/Pa]	2.0×10^{-7}	1.8×10^{-7}
T_m	[K]	558.0	548.0

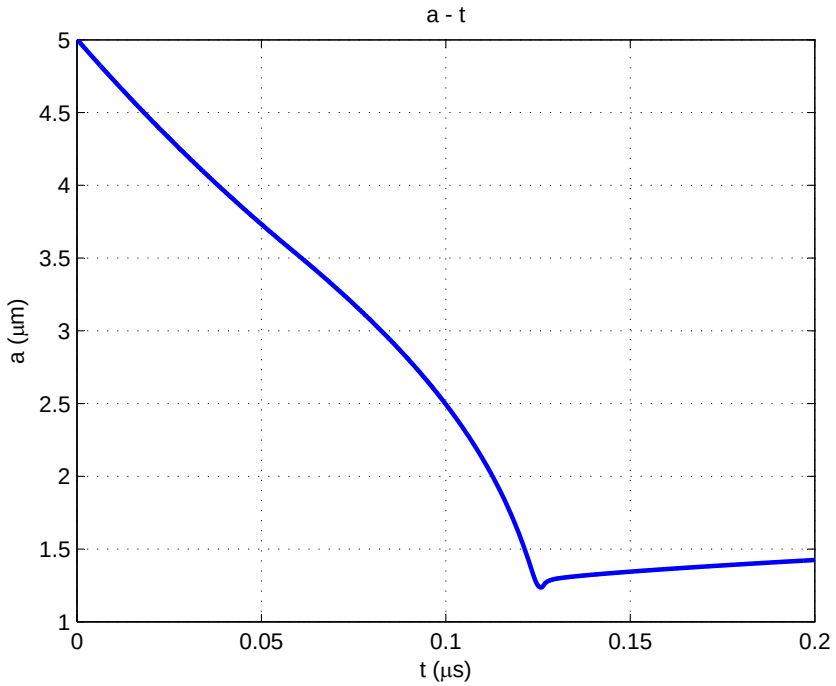

Figure 5.1: Variation of inner radius (RDX)

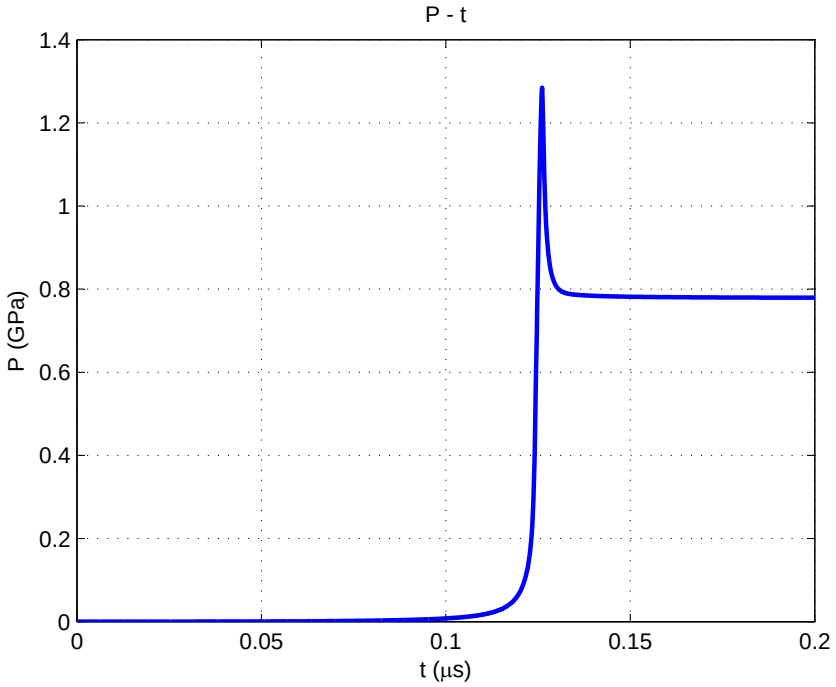

Figure 5.2: Variation of gas-phase pressure (RDX)

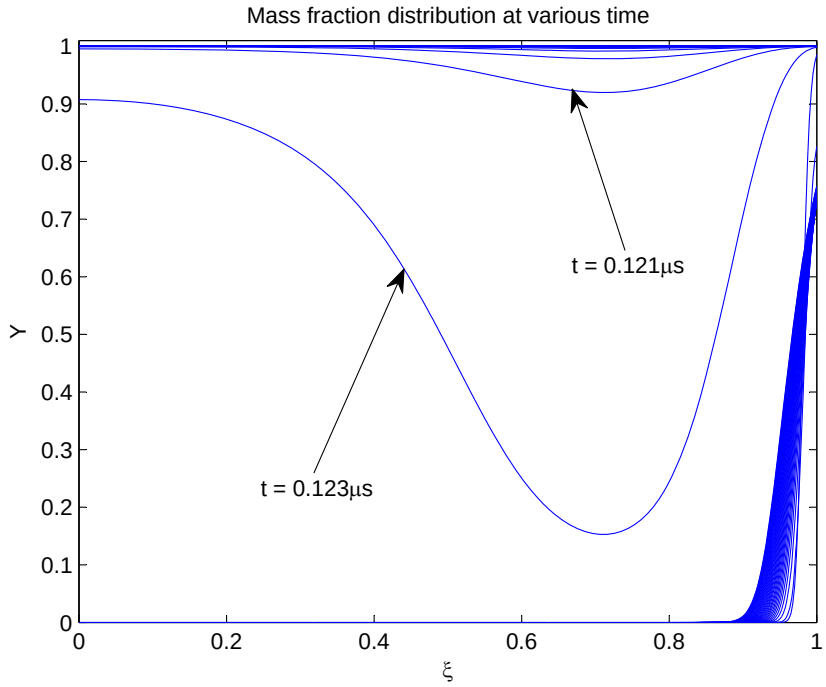

Figure 5.3: Variation of mass fraction distribution (RDX)

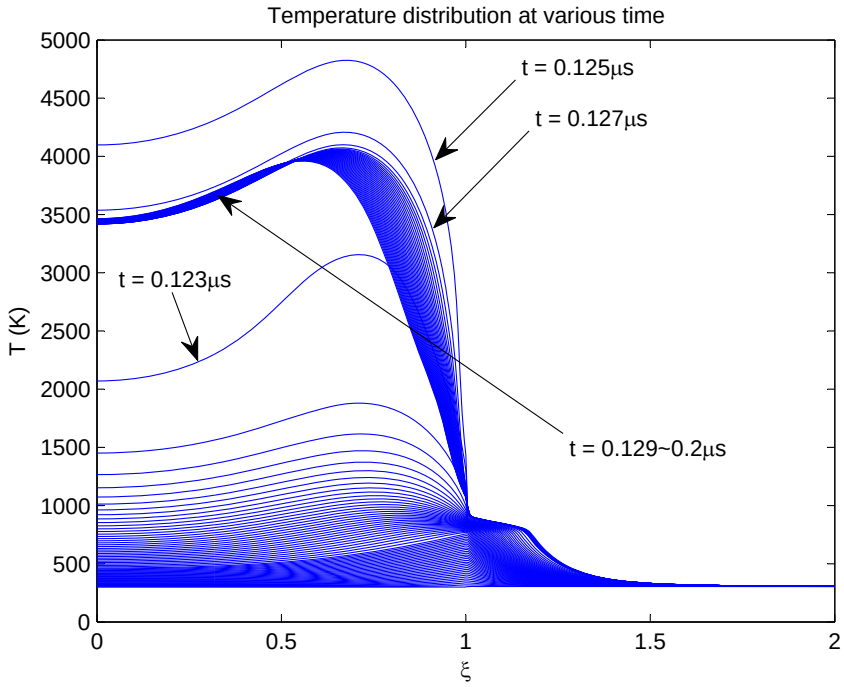

Figure 5.4: Variation of temperature distribution (RDX)

Given the initial conditions, a sustained shock of $P_s = 1$GPa is sufficient to initiate the pore collapse. During the initial time period $0 < t < 0.1\mu$s, the net resistive pressure, $P_g + P_y$, is less than the applied stress, P_s, and the pore collapses from the initial radius of $a_0 = 5\mu$m to $a = 2.5\mu$m generally.

As the pore collapses, viscous work and plastic work cause the interface temperature to increase and reach the condensed-phase melting temperature. From this point on the mass transfer is presented at the gas-phase-condensed-phase interface, and chemical reaction takes place inside the pore. The pore compression, mass transfer and chemical reaction cause the pore pressure and temperature increase steadily. However, the pore collapse is not terminated immediately at this point because the resistive pressure is still not large enough. Heat feedback from the gas phase to the condensed phase accelerates the consumption of energetic material at the interface. And it in return supports the chemical reaction within the void. As the mass transfer and chemical reaction continue, the pore pressure finally comes to an abrupt change. Over the time duration of less than $\Delta t \approx 10^{-3}\mu$s (estimated) at $t = 0.125\mu$s, P_g increases from 0.05GPa to around 1.3Gpa, where at approximately the same time, the pore collapse terminates and expansion begins. By this moment, the hot spot creation has been completed.

In the hot spot growth step that follows, the gas pressure decreases for a short duration, and then approach constant value. The pore continues expanding because of the mass transfer at the interface.

The temperature distribution and mass fraction distribution plots, Fig.(5.4) and Fig.(5.3), reveal more detailed information about the process. In Fig.(5.3), we can see that chemical reaction takes places around $t = 0.11\mu$s, much earlier than the pore reaches its minimal size. At this point, the gas-phase temperature is just around 1000K. However, in the following nano-seconds, the temperature distribution experiences an significant change, from 1,000K to around 4,500K, allowing the pore pressure to reach the point that starts the expansion. Because of the pore expansion, the pore temperature decreases for a short duration and finally stays a nearly constant stage, Fig.(5.4). In the process of pore deformation, the temperature at outer radius also varies with time. Since the viscous and yield heating sources are very weak at $r = b$, the temperature does not increase much.

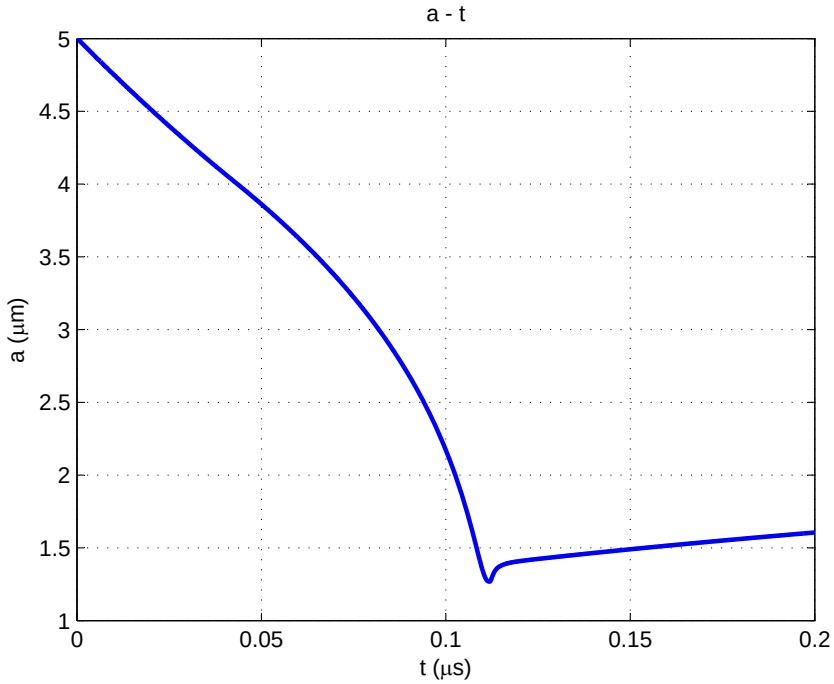

Figure 5.5: Variation of inner radius (HMX)

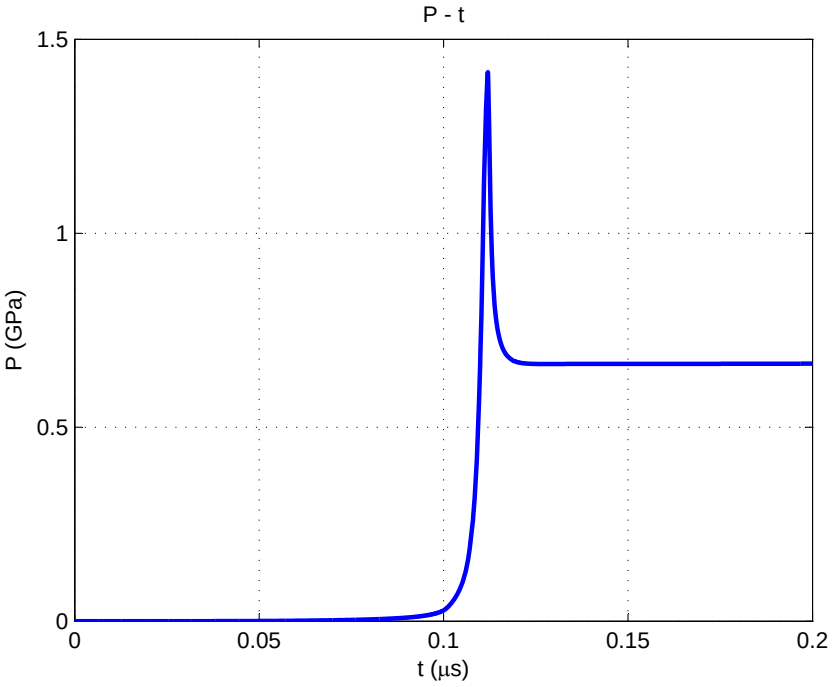

Figure 5.6: Variation of gas-phase pressure (HMX)

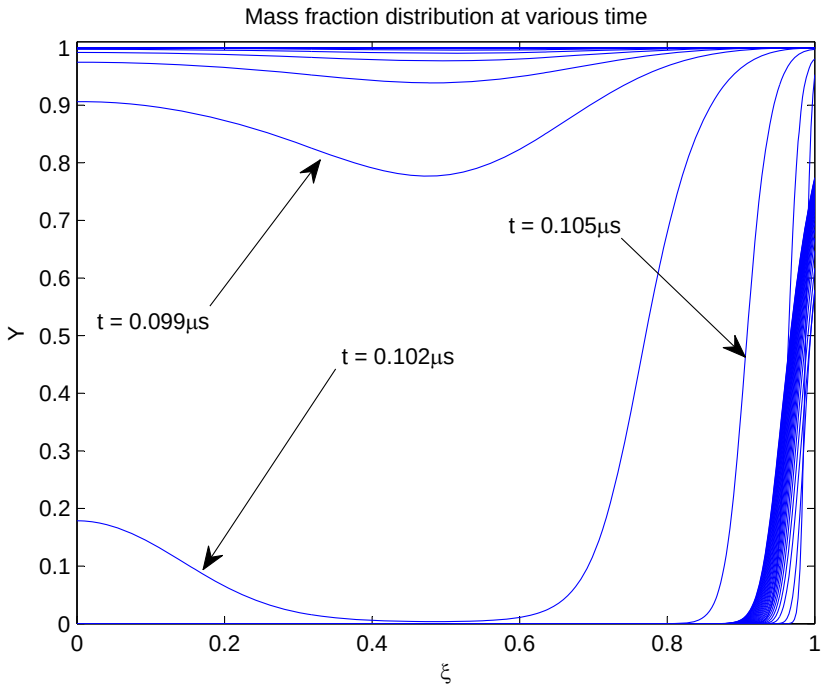

Figure 5.7: Variation of mass fraction distribution (HMX)

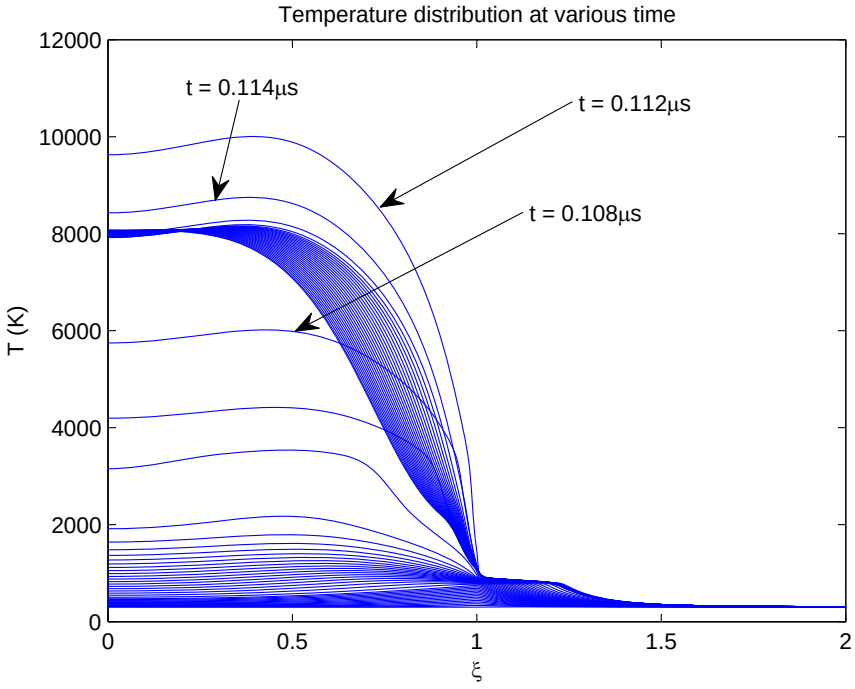

Figure 5.8: Variation of temperature distribution (HMX)

Fig.(5.5) - Fig.(5.8) present the numerical results of the discrete hot spot model using HMX as the surrounding material. Similar variations in pore size, pressure, mass fraction distribution and temperature distribution are obtained. The characteristic time scale is of the same order as it is in the RDX case. However, the induction time for HMX is about 0.01μs faster than RDX, and the instant maximum flame temperature goes beyond 10,000K, much higher than RDX's maximum flame temperature of 5,000K.

CHAPTER 6

CONCLUSION AND FUTURE WORK

This thesis studies the hot spot formation in condensed-phase, energetic materials under shock loading. Two models have been introduced based on the viscoplastic pore collapse model presented in Kang[22] and Massoni's[17] work.

Through a series of numerical experiments, it has been shown that viscoplastic heating is an effective mechanism in shock-induced hot spot generation in energetic material. The combination of viscous work heating and plastic yield work heating increases the temperature at the gas-phase-condensed-phase interface during the pore collapse process. It is also shown that the material's initial porosity and pore size have strong influences on the formation of hot spot. For given initial porosity and inner radius, the shock pressure must exceed a certain value to initiate a gas-phase reaction or make the pore to expand. Induction time decreases when the shock pressure keeps increasing, because the intensified viscoplastic heating effect, especially the viscous heating source, increases the interface temperature to its melting temperature in a shorter time. This decreasing trend is more significant for $1\text{GPa} < P_s < 5\text{GPa}$, and it becomes general when $5\text{GPa} < P_s < 9\text{GPa}$. The initial pore size also effects the hot spot generation. When combined with the effects of the material porosity, it makes the induction time to vary much at low shock loading, $1\text{GPa} < P_s < 3\text{GPa}$. In all cases, the time scale for hot spot generation stays at $O(10^{-7})$s, a reasonable agreement with the time scale of shock-to-detonation transition, $O(10^{-6})$s, in Ju and Jackson's work [25]. Once formed, the hot spot finally reaches a quasi-steady state, with the pore continuing expanding through consuming the interface material but the pressure and temperature stays nearly constant.

These contributions allow us to progress in the modeling of two/three-dimensional formation of hot spot in energetic material under shock initiation. Once the model is certificated in these cases, we can move on to

the building of a deterministic model for shock to detonation transition of condensed energetic materials.

REFERENCES

[1] C. J. Doolan, D. Science, and T. O. (Australia)., *A microstructure dependent reactive flow model for heterogeneous energetic materials / C.J. Doolan*. DSTO Systems Sciences Laboratory, Edinburgh, S. Aust. :, 2003.

[2] F. P. Bowden and A. F. Yoffe, *Initiation and Growth of Explosion in Liquids and Solds*. Cambridge University Press, Cambridge, 1952.

[3] J. E. Field, N. K. Bourne, S. J. P. Palmer, S. M. Walley, J. Sharma, and B. C. Beard, "Hot-spot ignition mechanisms for explosives and propellants [and discussion]," *Philosophical Transactions: Physical Sciences and Engineering*, vol. 339, no. 1654, pp. pp. 269–283, 1992.

[4] C. A. Forest, "Burning and detonation," Tech. Rep. LA-7245, Los Alamos National Laboratory Report, Los Alamos, New Mexico, 1978.

[5] E. L. Lee and C. M. Tarver, "Phenomenological model of shock initiation in heterogeneous explosives," *Physics of Fluids*, vol. 23, pp. 2362–2372, Dec. 1980.

[6] J. N. Johnson, P. K. Tang, and C. A. Forest, "Shock-wave initiation of heterogeneous reactive solids," *Journal of Applied Physics*, vol. 57, pp. 4323–4334, May 1985.

[7] R. Menikoff and M. S. Shaw, "Review of the forest fire model for high explosives," *Combustion Theory and Modelling*, vol. 12, no. 3, pp. 569–604, 2008.

[8] N. Whitworth, *Mathematical and NumericalModelling of Shock Initiation in Heterogeneous Solid Explosives*. PhD thesis, CRANFIELD UNIVERSITY, 2008.

[9] G. K. D.A. Jones and R. Borg, "Numerical simulation of detonation in condensed phase explosives," Tech. Rep. DSTO-TR-0705, Weapons Systems Division, Aeronautical and Maritime Research Laboratory, 1999.

[10] E. L. Lee and C. M. Tarver, "Phenomenological model of shock initiation in heterogeneous explosives," *Physics of Fluids*, vol. 23, no. 12, pp. 2362–2372, 1980.

[11] C. L. Mader, *Numerical Modeling of Detonations, Lod Alamos Series in Basic and Applied Sciences*. University of California Press, Berkeley, 1979.

[12] R. E. Setchell and P.A.Taylor, "The effects of grain size on shock initiation mechanisms in hexanitrostilbene (hns) explosive," *Prog. Astronaut. Aeronaut.*, vol. 94, p. 1984, 1984.

[13] R. B. Frey, "The initiation of explosive charges by rapid shear," (Annapolis, MD), in Proceedings of the 7th Symposium (International) on Detonation, 1981.

[14] Grady, D. E. and Kipp, M. E., "The growth of inhomogeneous thermoplastic shear," *J. Phys. Colloques*, vol. 46, pp. C5–291–C5–298, 1985.

[15] M. E. Kipp, "Modeling granular explosive detonations with shear band concepts," (Albuquerque, NM), pp. 35–41, in Proceeding of the 8th Symposium (International) on Detonation, 1985.

[16] M. M. Chaudhri, "Slab initiation of explosives," *Nature*, vol. 263, 1976.

[17] J. Massoni, R. Saurel, G. Baudin, and G. Demol, "A mechanistic model for shock initiation of solid explosives," *Physics of Fluids*, vol. 11, pp. 710–736, Mar. 1999.

[18] M. M. Carroll and A. C. Holt, "Static and dynamic pore-collapse relations for ductile porous materials," *Journal of Applied Physics*, vol. 43, no. 4, pp. 1626–1636, 1972.

[19] A. C. H. M. M. Carroll and B. M. Butcher, "Application of a new theory for the pressure-induced collapse of pores in ductile materials," tech. rep., in Proceeding of the International Symposium on Pore Structure and Properties of Materials, Prague, 1973.

[20] L. Rayleigh, "Viii. on the pressure developed in a liquid during the collapse of a spherical cavity," *Philosophical Magazine Series 6*, vol. 34, no. 200, pp. 94–98, 1917.

[21] B. B. A. Khasinov, A. A. Borisov and A. I. Korotkov, "Two-phase viscoplastic model of shock initiation of detonation in high density pressed explosives," (Annapolis, MD), pp. 435–447, in Proceeding of the 7th Symposium (International) on Detonation, 1981.

[22] J. Kang, P. Butler, and M. Baer, "A thermomechanical analysis of hot spot formation in condensed-phase, energetic materials," *Combustion and Flame*, vol. 89, no. 2, pp. 117 – 139, 1992.

[23] D. L. Bonnett and P. B. Butler, "Hot-spot ignition of condensed phase energetic materials," *Journal of Propulsion and Power*, vol. 12, no. 4, pp. 680–690, 1996.

[24] Y. Hamate and Y. Horie, "Ignition and detonation of solid explosives: a micromechanical burn model," *Shock Waves*, vol. 16, no. 2, pp. 125–147, 2006.

[25] J. Zhang, T. L. Jackson, J. D. Buckmaster, and J. B. Freund, "Numerical modeling of shock-to-detonation transition in energetic materials," *Combustion and Flame*, vol. 159, no. 4, pp. 1769 – 1778, 2012.